ABSTRACT

ALEJANDRO VALENCIA: Title : Assessment of the Relative Reduction Factor for an Ozone Attainment Demonstration in Houston, Texas. (Under the direction of William G. Vizuete.)

The Houston/Galveston/Brazoria (HGB) area has been designated as a non-attainment area for the 8-hour ozone (O_3) National Ambient Air Quality standard (NAAQS) set by the U.S. Environmental Protection Agency (EPA). The Texas Commission of Environmental Quality is currently creating a State Implementation Plan to show future attainment following the EPA's guidance document. The guidance describes how to apply air quality models (AQMs) to generate the predictions later used to evaluate O_3 attainment. Predictions from AQMs are used in a "relative" respect, rather than in an "absolute" sense by calculating the relative reduction factor, or RRF . The RRF is a ratio of future year to current year average predicted O_3 at a given monitor. The main goal of this study is to understand the implications of the averaging technique for calculating the RRF. To assess variability in RRF, this study quantifies the sensitivity of O_3 production to changes in precursor concentrations due to human activity throughout the week and to recurring meteorological phenomena in the rise of the simulated planetary boundary layer. At any given monitor, up to 40% of the days used RRF calculations that included these phenomena. Consequently, modeling days were included where O_3 concentrations and RRFs can vary by as much as 35 ppb and 0.07, respectively. This introduces a margin of error that can determine the attainment or lack thereof in the HGB area.

ACKNOWLEDGMENTS

This paper would not have been possible without guidance of my advisor William Vizuete, and the members of the UNC Modeling Air Quality (MAQ) and Climate Health and Air Quality (CHAQ) Lab. This project was funded by the Housotn Advanced Research Center (HARC) under Project H97.

TABLE OF CONTENTS

LIST OF TABLES

LIST OF FIGURES

LIST OF ABBREVIATIONS AND SYMBOLS

AQM	Air Quality Models
BPA	Beaumont-Port Arthur modeling domain
CAA	Clean Air Act
CAMS	Continuous Ambient Monitoring Stations
CAMx	Comprehensive Air quality Model with extensions
CBIV	Carbon Bond IV chemical mechanism
CB05	Carbon Bond '05 chemical mechanism
CCEDS	Consolidated Compliance and Enforcement Data System
CHOU	Central Houston
CMAQ	Community Multiscale Air Quality model
CO	Carbon monoxide
DV	Design Value
DV_B	Base line Design Value
DV_F	Future Design Value
EI	Emission Inventory
EPA	U.S. Environmental Protection Agency
ETH	Ethene
ETX	Eastern Texas 12-km subdomain
FORM	Formaldehyde
H_2O_2	Hydrogen Peroxide
HGB	Houston/Galveston/Brazoria
HNO_3	Nitric Acid
HONO	Nitrous acid
HRVOC	Highly Reactive Volatile Organic Compound
IPR	Integrated Process Rate
IRR	Integrated Reaction Rate

k_v	vertical layer interface diffusivity
LST	Local Standard TIme
MCIP	Meteorology-Chemistry Interface Processor
MM5	Mesoscale Model version 5
MMV	Model Mixing Volume
NAAQS	National Ambient Air Quality Standard
NCAR	National Center for Atmospheric Research
NO	Nitric oxide
NO_x	Nitrogen Oxide
O_3	Ozone
$^{\cdot}OH$	Hydroxyl Radical
OLE	CBIV model olefin species
PA	Process Analysis
PAR	CBIV model parafin species
PBL	Planetary Boundary Layer
PSU	Pennsylvania State University
ppm	Parts per million
ppb	Parts per billion
pyPA	Python Process Analysis post-processing suite
REG	Regional 36-km subdomain
RRF	Relative Reduction Factor
$S_{B,m,d}$	base line predicted max 8-hr O_3 concentrations "near" each monitor
$S_{F,m,d}$	future predicted max 8-hr O_3 concentrations "near" each monitor
$\overline{S_{B,m}}$	mean base line predicted max 8-hr O_3 concentrations
$\overline{S_{F,m}}$	mean future predicted max 8-hr O_3 concentrations
SETPMTC	Southeast Texas Photochemical Modeling Technical Committee

SIP	State Implementation Plan
TLL	Tank Landing Loss
TCEQ	Texas Commission of Environmental Quality
UNC-CH	University of North Carolina at Chapel Hill
UH	University of Houston
VOC	Volatile Organic Compound
VOCC	Volatile Organic Compound carbon

CHAPTER 1

INTRODUCTION

Ozone (O_3) is one of the main components of smog, air pollution. O_3 in the stratosphere benefits the environment by filtering potentially harmful ultraviolet rays from reaching the Earth's surface. Troposheric or surface-level O_3, however, has been linked with deteriorating ecosystems and human health (EPA, 2008b). The Clean Air Act (CAA) protects human health and welfare by requiring the Environmental Protection Agency (EPA) to establish the National Ambient Air Quality Standards (NAAQS). In 1997, the EPA set an 8-hour (8-hr) O_3 standard for ambient air at 0.080 ppm. In 2008, however, the 8-hr O_3 standard was changed to 0.075 ppm. The 1997 standard remains in place until EPA commences a rulemaking to address a transition between standards. For an area to be designated "in attainment" of the NAAQS for O_3, the three-year average of the fourth highest daily 8-hr maximum O_3 concentration for each of the three years must not exceed 0.08 ppm (EPA, 2008a). In 2004, over 100 million people in the US resided in areas exceeding the 8-hr O_3 standard (ALA, 2004). These "non-attainment" areas must produce an attainment demonstration State Implementation Plan (SIP) according to Section 182 of the 1990 CAA Amendments or have their federal highway funding removed and face other sanctions. The SIP describes the steps the state will take to reduce O_3 concentrations.

O_3 is not directly emitted into atmosphere, and thus it is considered a secondary air pollutant. It is formed through complex meteorological and chemical processes. These chemical processes require nitrogen oxides (NO_x) and volatile organic compounds (VOC). Reducing the concentration of such precursors is the only means

policy makers have to control O_3. To assess the proposed emission reduction strategies, policy makers must rely on air quality models (AQMs). Using meteorology, emissions and chemistry data as inputs, these models simulate production and transport of secondary air pollutants. Output from the simulation is used to evaluate the efficacy of emissions reduction controls as delineated in the region's SIP.

The Houston/Galveston/Brazoria (HGB) area is an example of a region currently creating a SIP to show future attainment. Houston exceeds the NAAQSs for O_3 and has been designated as a severe O_3 non-attainment area by the EPA (TCEQ, 2004). The American Lung Association ranked the Houston-Baytown-Huntsville metropolitan statistical area as the fifth most O_3 polluted in the nation (ALA, 2007). Major sources in Houston include oil and petrochemical industries and a significant mobile emission sector. The mixture of industrial plants, the substantially trafficked highway system, and the areas unique meteorology make Houston's conditions ideal for high ozone concentrations.

A focus of this modeling investigation is to understand the causes of high O_3 in Houston and their impact on showing attainment of the federal O_3 standard. Thus, it is useful to summarize the EPA guidance on the use of AQM predictions and observational data to show attainment of the O_3 NAAQS. The basic equation that the EPA guidance establishes to carry out model attainment tests per monitor is eq. 1.1.

$$DV_{F,m} = DV_{B,m} \times RRF_m \tag{1.1}$$

where $DV_{B,m}$ is the base line design value for monitor m (based on monitor observations), RRF_m is a relative reduction factor for monitor m (based on model predictions), and $DV_{F,m}$ is the future design value in the attainment year for monitor m. Regional

attainment is achieved when all monitors within the region have $DV_{F,m}$ values less than or equal to 84 ppb. A detailed explanation of each term follows in this section.

In brief, attainment is determined by a combination of observations and AQM predictions. The EPA guidance's methodology to assess observed data consists of calculating a "base line" design value or DV_B. To calculate a DV_B, the policy maker must first decide on a base line year. Typically, this year coincides with the year being simulated by the regulatory AQM. Once a base line year is chosen, there are four methodologies described in the guidance for calculating a DV_B (EPA, 2007). For the modeled attainment tests, the EPA guidance recommends to calculate a DV_B consisting of the average of three 8-hr O_3 regulatory design values (DV_m), which straddle a base line inventory year (EPA, 2007). This method (the five year, weighted-center method) for calculating a DV_B, is shown in equation (1.2) for the base line year y

$$DV_{B,m,y} = \frac{DV_{m,y-1} + DV_{m,y} + DV_{m,y+1}}{3} \tag{1.2}$$

where the (DV_m) of a monitor is an *observational-based average* used to determine whether a region is in attainment (EPA, 2008a). The 8-hr O_3 DV_m is calculated as the 3-year average of the fourth highest monitored daily 8-hr maximum value at each monitoring site. A detailed description of the methodology to calculate a DV_m can be found in 40 CFR Part 50.10, and Appendix I to Part 50 (EPA, 2008a).

The guidance further describes the use of models for determining the reduction factor that can be applied to the DV_B. According to the EPA, when creating model simulations, three sets of emission inventories (EI) are required, base case, base line and future case. The base case uses day-specific emission rates in an attempt to accurately replicate the specific period. For this reason, the base case EI is used in

the model performance evaluation. After the performance evaluation, the EI should correspond with the base line year chosen in the DV_B. Moreover, the EPA guidance states that this EI must be modified to include only "typical" emissions. Therefore, the base line inventory may need to replace the day specific emissions with average or "typical" emissions for certain types of sources. Consequently, the base line EI forms the basis for the 2018 EI. The EI for 2018 includes all existing emissions controls, projected growth of emissions, and proposed emission controls.

Once the simulations have been created, the produced data are used in a "relative" respect, rather than in an absolute sense, as stated by the EPA (EPA, 2007). This method uses modeled data to calculate the relative response factor (RRF) for every monitor to demonstrate attainment. This is accomplished by selecting "qualified" maximum 8-hr O_3 model predictions "near" each monitor, m, for each model episode day, d, in the base line simulation ($S_{B,m,d}$), and the highest model prediction "near" the same monitor for the same episode day in a future simulation ($S_{F,m,d}$). Using these values, equations (1.3) and (1.4) show how each monitor's mean base line ($\overline{S_{B,m}}$) and mean future ($\overline{S_{F,m}}$) predicted maximum 8-hr O_3 concentrations are calculated over all modeled days, given a "sufficient number" of days, D, of "qualified" values near monitor m.

$$\overline{S_{B,m}} = \frac{\sum_{d=0}^{D} S_{B,m,d}}{D} \tag{1.3}$$

$$\overline{S_{F,m}} = \frac{\sum_{d=0}^{D} S_{F,m,d}}{D} \tag{1.4}$$

The RRF_m for the monitor m is defined in equation (1.5).

$$RRF_m = \frac{\overline{S_{F,m}}}{\overline{S_{B,m}}} \tag{1.5}$$

Equation (1.5), however, does not stand alone. The guidance establishes several procedures that should be followed when calculating a RRF_m to reduce uncertainty. Specifically, it indicates the criteria for determining a "qualified" prediction, how to choose a prediction "near" a monitor, and what are "sufficient" numbers of days required for this calculation. These procedures are described below.

When determining "qualified" predictions, the guidance documents suggest limiting the $S_{B,m,d}$ chosen to calculate RRF_m. Given that modeled meteorological conditions may cause under-prediction of O_3 at a given monitor site, the modeled predictions for that day may be unresponsive to controls and over estimate the DV_F projection. Thus, the guidance recommends a minimum concentration threshold of 85 ppb. This will results in less uncertainty and more robust RRF_m and DV_F (EPA, 2007).

To find predictions "near" a monitor, the EPA guidance states that the location of $S_{B,m,d}$ and $S_{F,m,d}$, should be searched for in a radius up to 15 km away from monitor m. According to the guidelines, this is to account for model inaccuracy in correctly predicting the location of peak O_3 (EPA, 2007). Thus, it is suggested by EPA guidance to expand the selection of the $S_{B,m,d}$ value to include an array of grid cells that surround a monitor, rather than limiting the selection to the grid cell where the monitor is located.

Finally, a minimum of 10 "qualified" values "near" the monitor, or $S_{B,m,d}$ is strongly recommended by the EPA. This is based on an assumption that this increases the stability of the RRF (EPA, 2007). If the episode(s) did not predict enough modeling days with $S_{B,m,d}$ greater than 85 ppb, then the minimum threshold can be reduced to,

but never below 70 ppb. If relatively few ozone days are being modeled or certain monitors have relatively few exceedances (above 70 ppb), then it is recommend to use an absolute minimum number of 5 days in the calculation. If the base line model predictions did not result in at least 5 days with a $S_{B,m,d}$ above 70 ppb near a monitor, then the monitor is excluded from the RRF_m calculation. The guidance states that if there are fewer than 5 days available for RRF_m calculations at monitoring sites that are above the NAAQS, the appropriate U.S. EPA Regional office should be consulted.

The above criteria do not take into consideration how emissions and meteorology are directly related to O_3 production and can therefore bias the RRF_m. For example, the model's EI (both base case and base line) simulates daily variance in O_3 precursors to reflect human activity. In weekends, when emissions of anthropogenic precursors, (NO_x and VOC) are the lowest, several studies have observed peak O_3 concentrations in urban areas of North America and Europe (Pryor and Steyn, 1995; Vukovich, 2000; Pont and Fontan, 2001; Pun et al., 2003). Other sites in rural areas or regions with high biogenic VOC emissions show that O_3 reaches a minimum during the weekend (Husar, 1998; Heuss et al., 2003). AQMs simulating day-of-the-week phenomena have predicted large differences in O_3 between weekdays and weekends (Vukovich and Scarborough, 2004; Yarwood et al., 2008). Moreover, a study of the weekend effect on observed O_3 in several metropolitan areas shows that Houston has the greatest increase in O_3 during the weekend (Blanchard et al., 2008). Additionally, simulations of the HGB predict varying O_3 due to day-of-the-week phenomena (Smith et al., 2007).

In addition to neglecting the day-of-the-week effect, the EPA guidance averaging technique fails to account for recurring meteorological events that influence O_3 production. A study of the well-mixed air directly above the earth's surface, or planetary boundary layer (PBL), in the model has shown that changes in the chemical system

that changes the conditions in which ozone is produced occur with varying simulated PBL heights (Vizuete et al., 2007).

In brief, the EPA guidance relies on averaging techniques that were intended to reduce the variability resulting from uncertainty in the modeling system. Several modeling studies, however, have focused on the effect of changes in modeling systems and model inputs on the variability of RRF_m. An investigation by Sistla et al., 2004 found variations in DV_F of 35 ppb resulting from the selection of emission inventories and different photochemical AQMs. In a separate study, Jones et al., 2005 identified uncertainties in DV_F of 24 ppb stemming from choice of meteorology model and chemical mechanism. More recently, Hogrefe et al., 2008 found that RRF_m values were insensitive to changes in model performance in his model conditions. All modeling predictions used in these studies used horizontal grid spacing of 12-km. Therefore, all O_3 precursor emissions were automatically dispersed within a 12-km^2 grid cell, effectively preventing any sharp gradients in NO_x, VOC, or O_3 concentrations. This smoothing of concentration gradients prevented the model from producing O_3 in NO_x inhibited environments, or from concentrated plumes of VOC. Thus, the attainment methodology described by the EPA has yet to be fully evaluated in an environment of heterogenous gradient of emissions, or for a simulation set used for an actual SIP.

The main goal of this study is to understand the implications of the averaging technique for calculating the RRF_m focusing on an simulation set used for a SIP. The investigation quantifies the sensitivity of O_3 production to changes in precursor concentrations due to human activity and simulated PBL. The findings from this study first describe the phenomenon that cause fluctuations of O_3 due to day-of-the-week effects and their implications for attainment metrics. Next, details of simulated PBL behavior and their influence on attainment metrics are depicted in the meteorology

analysis results. Finally, to understand the modeling system conditions of O_3 production, a study of the magnitudes of physical and chemical processes of the simulated PBL trends are described in the process analysis results.

CHAPTER 2

METHODOLOGY

2.1 Air Quality Model Dataset

The air quality model dataset used in this study spans several years and was generated by researchers at the University of Houston (UH) and Texas state regulators. The Texas Commission on Environmental Quality (TCEQ) used the Comprehensive Air Quality Model with Extensions (CAMx) version 4.31, and developed a 2000 episode to support regulatory decisions for attainment of the federal O_3 standard (ENVIRON, 2005). The TCEQ also developed regulatory simulations using CAMx version 4.51 for 2005, 2006, and 2018. A second 2006 simulation was completed by UH to support scientific inquiries using the Community Multi-scale Air Quality (CMAQ) version 4.4 (EPA, 2006). Details concerning the development of the UH EIs, meteorology, domain configurations, and model performance can be found on the UH website (Byun, 2007) and in the UH H87 final technical report (Byun et al., 2007) for the Houston Advanced Research Center (HARC). The dates covered by all these simulations are shown in Table 2.1. The combination of these regulatory and scientific modeling episodes results in 413 modeling days of southeast Texas. The TCEQ simulations for 2005 and 2006 will be the focus of this study and will now be discussed with more detail.

The TCEQ prepared the CAMx simulations to support their attainment demonstration of the federal standard for O_3 in the HGB non-attainment area. A CAMx simulation of the summer of 2000 and was used as the basis for regulations adopted in the 2004 1-hr O_3 SIP (TCEQ, 2004). Details on the 2000 episode can be found

on the TCEQ website (TCEQ, 2009b). In support of the upcoming 2010 8-hr O_3 SIP, the TCEQ created the 2005, 2006, and 2018 episodes, which are the focus of this investigation. As shown in Figure 2.1, these simulations used a regional 36-km domain (REG), 12-km Eastern Texas (ETX) domain, and a 4-km Houston Galveston Beaumont Port Arthur (HGB/BPA) domain (TCEQ, 2005). A 2-km domain was also developed centered on the the Houston urban region. As shown in Figure 2.1, all horizontal domains used the same vertical structure, where the ground layer is 34 meters thick and each vertical layer is less than 100 meters thick until layer 11. Appendix A contains more specific details about each domain.

For the 2005 and 2006 episodes the TCEQ created meteorological inputs using the PSU/NCAR mesoscale model (MM5) (Grell et al., 1995) and have named these files "eta_dbemis_fddats_uhsst_utcsrlulc.v45.TKE," as shown in Table 2.1 (Details in Appendix A). The EIs for these two episodes were generated following EPA guidance, and included the creation of two sets of EIs named the base case and base line. The base case files provided by the TCEQ were named "reg8" and base line files "reg1" as shown in Table 2.1. The main difference between these EIs lies in spatial and temporal allocation of emissions; refer to section 1. The implementation of the base line simulation by the TCEQ resulted in several changes in the EI. Adjustments were made to point sources to exclude any day-specific information. This is compromises by removing the Special Inventory and the Consolidated Compliance and Enforcement Data System (CCEDS) dataset, which consist of a compilation of emission events of excess precursors. In addition, the Hourly Tank Landing Loss (TLL) emissions and diurnal profiles were removed and replaced with averaged values. The rest of the inventory remained the same including biogenic emissions, area and non-road mobile, on-road mobile emission sources, and Highly Reactive Volatile Organic Compounds (HRVOC) emission rates. HRVOCs are defined in the Texas SIP as the

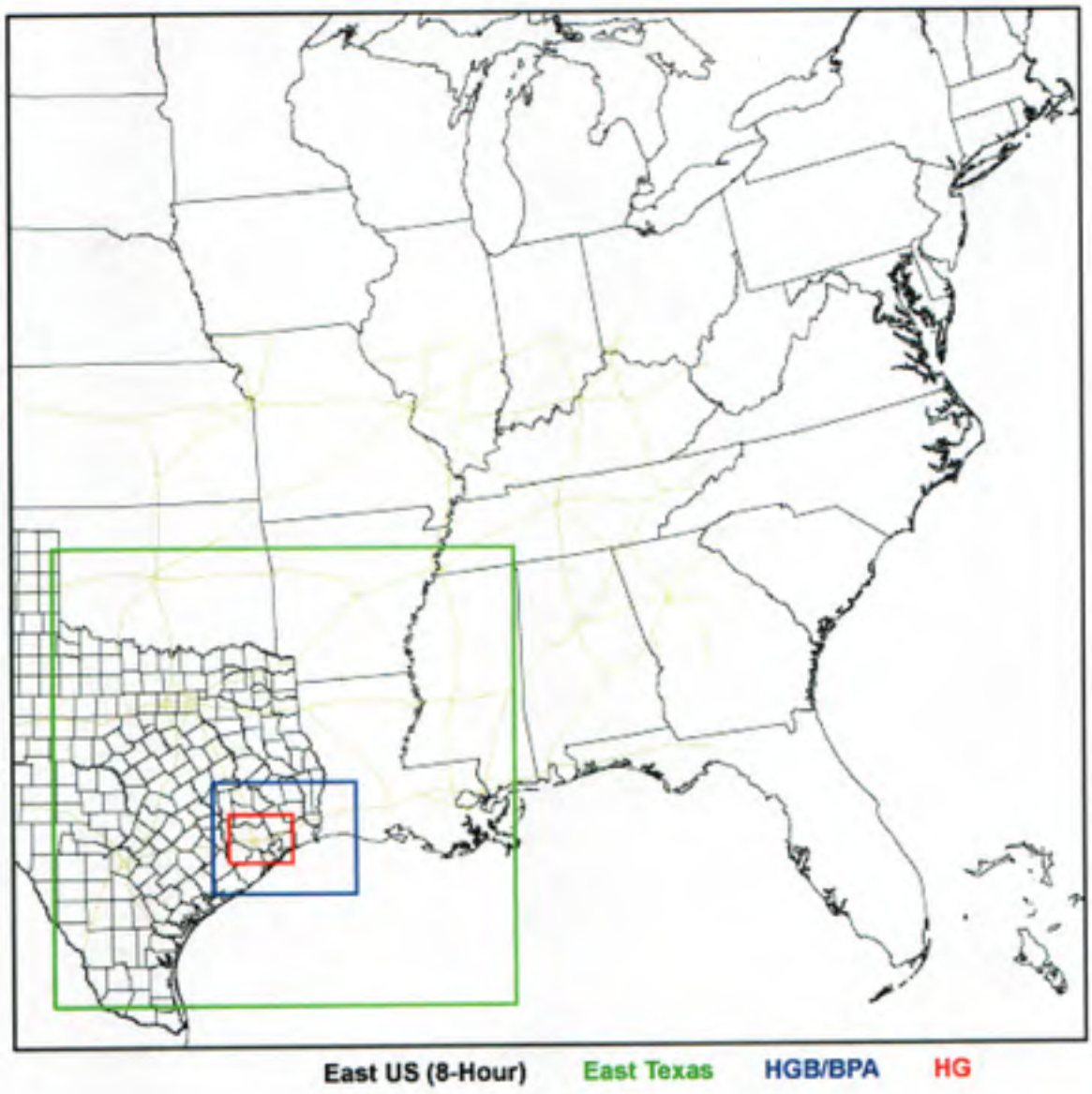

Figure 2.1: Horizontal modeling domains for the TCEQ 2005, 2006, and 2018 simulations..The Regional 36-km coarse grid (blue boundary), the East Texas 12-km grid (green), the Houston Galveston Brazoria Beaumont Port Arthur 4-km grid (blue), the Houston Galveston 2-km grid (red)

Table 2.1: Southeast Texas air quality modeling episodes created by the TCEQ in support of ozone SIPs, and the air quality modeling episode developed by UH.

Developer	Model Software	Simulation Period	EI File Name		Met. File Name	Chemical Mechanism	Received
			Base Case	Basline			
TCEQ	CAMx v4.31	2000-08-16 to 2000-09-06	pscfolev1	N/A	TCEQuh1_eta	CBIV	2000-08-16
	CAMx v4.51	2005-05-19 to 2005-06-03	reg8	reg1	eta_dbemis_fddats_uhsst_utcsrlulc.v45.TKE	CB05	2008-11-12
		2005-05-17 to 2005-06-30					
		2005-07-26 to 2005-08-08					
		2006-05-31 to 2006-06-15					2008-12-05
		2006-08-13 to 2006-09-15	reg8si				
		2006-09-16 to 2006-10-11	reg8				
UH	CMAQ v4.4	2006-08-16 to 2006-09-15	BEMR	N/A	uhTMNS11n2	CBIV	2008-05-15
TCEQ	CAMx v4.51	2005-05-19 to 2005-06-03	N/A	cs02	eta_dbemis_fddats_uhsst_utcsrlulc.v45.TKE	CB05	2008-11-12
		2005-05-17 to 2005-06-30					
		2005-07-26 to 2005-08-08					
		2006-05-31 to 2006-06-15					
		2006-08-13 to 2006-09-15					
		2006-09-16 to 2006-10-11					

N/A = Not applicable
TCEQ=Texas Commission on Environmental Quality
UH=University of Houston
CBIV=Carbon Bond Mechanism version 4
CB05=Carbon Bond Mechanism version 5

olefins: ethylene, propylene, butenes, and 1,3-butadiene (Allen et al., 2004). Since only ethene is explicit in the model, model HRVOCs were classified as carbon species ETH and OLE. More detailed information on the distinction between base line and base case for these simulations is available in HGB Modeling Update - 2005 Base line Emissions from the Southeast Texas Photochemical Modeling Technical Committee (SETPMTC) (Thomas, 2008). It is important to emphasize that the base line predictions, not the base case predictions, are used with predictions in the future case to calculate the RRF_m.

In addition to being used in the attainment demonstration, the base line EI forms the basis for the 2018 EI. The EI for 2018 includes all existing emissions controls, projected growth of emissions, and proposed emission controls. After precursor reduction with population growth (Fig. 2.2 (Karp, 2008)), overall NO_x is reduced by almost 40%. On-road emissions were reduced from 222 tpd to 50 tpd, a reduction of 78%. In the base line EI, the on-road NO_x emission were the largest contributor of emissions, 37%, however, after controls, the 2018 on-road emissions are only 14% of

all NO_x emissions. In 2018, point and non-road emission both decrease by around 20% while area NO_x emissions actually increase by 16%. The highest contributors of NO_x in the future case are point emissions with 43% of total NO_x followed by area emissions with 32%. Like NO_x, other heavily controlled precursors were VOCs. On-road, non-road, and point emission decreased each by 53%, 21% and 12%, respectively. Area VOC emissions, however, increased by 24%. Overall, VOCs increased from base line to future case by 2%. Detailed documentation regarding the development of this future year, base case, and base line EIs, and other modeling inputs can be found on the TCEQ website (TCEQ, 2009d).

After receiving all the necessary simulations, the raw modeling data was processed for analysis using code from the University of North Carolina at Chapel Hill (UNC-CH) to allow meaningful visualization of model inputs and outputs. Such preprocessing was mainly performed on base case simulaitons. In fact, the majority of the results presented here use model predictions based on the base case EI, not the base line EI. This was primarily due to our need to focus our investigation on modeling data without the averaging of emissions found in the base line inventory. In our analysis of impacts on RRF_m , however, the model predictions using the base line emissions and using the 2018 emissions were used to calculate a RRF_m following the EPA guidance (EPA, 2007).

2.2 Attainment Demonstration Average Statistics

In 2006, the HGB non-attainment area had 88 surface monitors taking measurements. Of these surface monitors, 25 were used by the TCEQ for their SIP DV_F calculations, and thus are the focus of this study. A list of the monitors is reported in Table 2.2, and and their locations are shown in Figure 2.3. In December 2008, we received from the TCEQ the 8-hr O_3 values for all 25 of these monitors used to

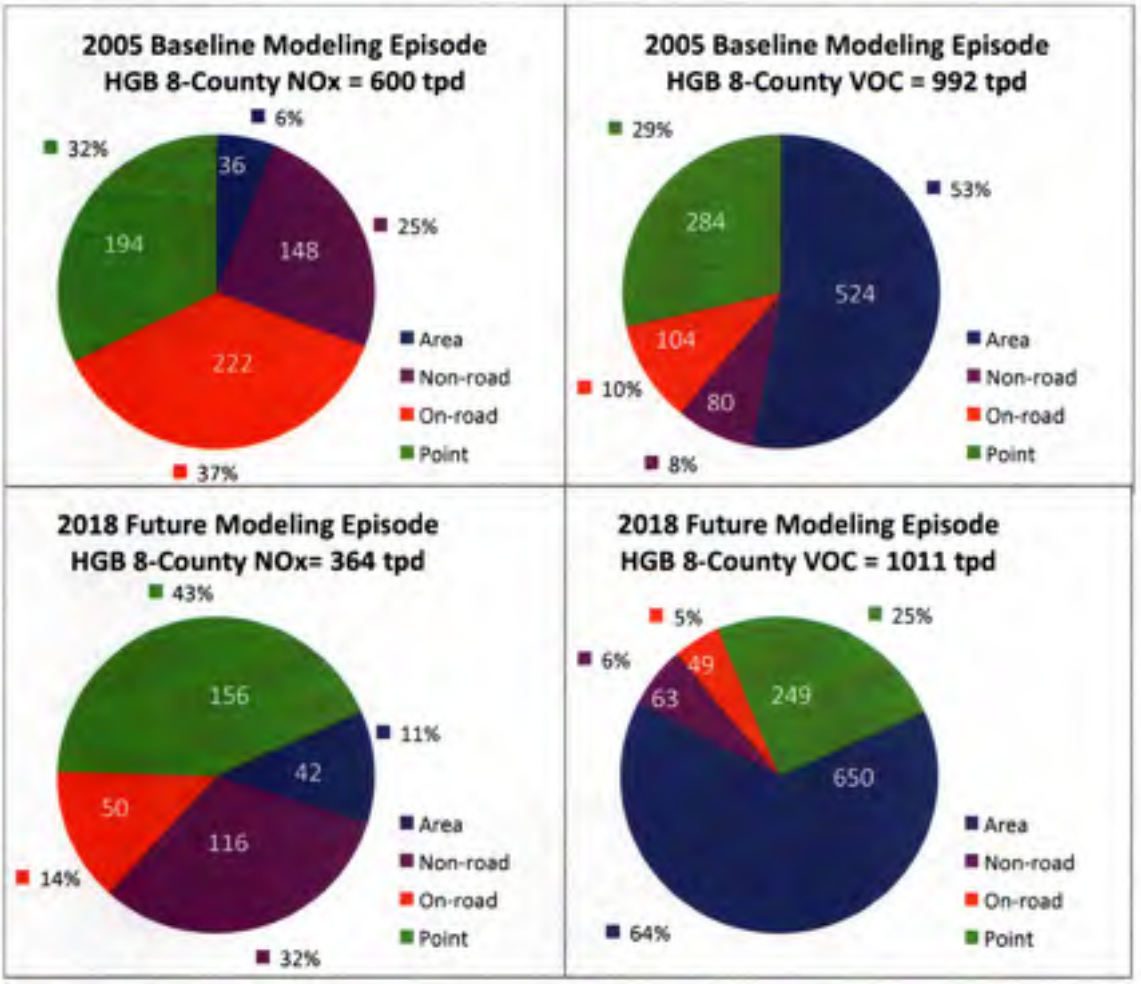

Figure 2.2: VOC and NO_x emissions (TPD) for 2005 base line emission inventory and 2018 emission inventory. D. Karp. Initial 2018 HGB modeling results. Presentation made November 3, 2008 (Karp, 2008).

calculate DV_{2005}, DV_{2005}, and DV_{2018}. The TCEQ also provided us with their RRF_{2005} values also shown in Table 2.2 and based on modeling predictions using a 2005 base line EI. Each monitor has an RRF_{2005} based on an average of multiple modeling days which range from 15-35 days as shown in Table 2.2. In this table, the monitors BAYP, HSMA, DRPK and WALV represent unique challenges to SIP modeling for showing O_3 attainment. According to TCEQ, the calculated DV_Fs for each are above 85 ppb (using 2005 as the base line year). These monitors have failed to demonstrate future

Table 2.2: Monitors in the HGB non-attainment region used in the TCEQ attainment demonstration. Listed in the table are the abbreviation of the monitor (Site), the unique identifying number for the Continuous Ambient Monitoring Station (CAMS), the name of the monitor, and attainment average statistics using a 2005 baseline (Baseline Design Value (DV_B), Relative reduction factor ($RRF_)$ and Future Design Value (DV_F)). This data was generated by the TCEQ and received on December 2008.

Site	CAMS	$DV_{B,2005}$ ppb	RRF_{2005} days	RRF_m	$DV_{F,2018}$ ppb
SHWH	Westhollow Houston	92.3	30	0.840	77
BAYP[1]	Bayland Park	100.7	33	0.861	86
HLAA	Houston Lang	78.7	30	0.857	67
HCQA	Houston Croquet	93.0	32	0.856	79
HTCA	Houston Texas Avenue	83.3	26	0.910	75
HALC	Houston Aldine	88.0	22	0.883	77
HROC	Houston Regional Office	84.3	25	0.919	77
HWAA	Houston North Wayside	78.7	21	0.902	70
HSMA[1]	Houston Swiss & Monroe	95.3	35	0.894	85
C35C	Clinton	86.3	27	0.925	79
HOEA	East Houston	82.7	25	0.922	76
H03H	HRM Site 3 Haden Road	88.0	25	0.934	82
DRPK[1]	Deer Park	96.3	27	0.922	88
HCHV	Houston Channelview	85.7	21	0.939	80
LYNF	Lynchburg Ferry	89.0	21	0.947	84
SBFP	Seabrook Friendship Park	89.3	19	0.919	82
WALV[1]	Wallisville Road	94.0	15	0.925	86
DNCG[2]	Danciger	81.5	9	0.851	69
HNWA[2]	NW Harris Tomball	91.7	21	0.842	77
LKJK[2]	Lake Jackson	77.5	12	0.872	67
CNR2[2]	Conroe	85.0	10	0.855	72
MACP[2]	Manvel Croix Park	94.7	33	0.866	81
MSTG[2]	Mustang Bayou	88.7	14	0.877	77
TXCT[2]	Texas City	87.7	21	0.918	80
GALC[2]	Galveston	85.0	20	0.922	78

[1] Monitors under non-attainment

[2] Monitors 25 km outside Downtown Houston Area

attainment.

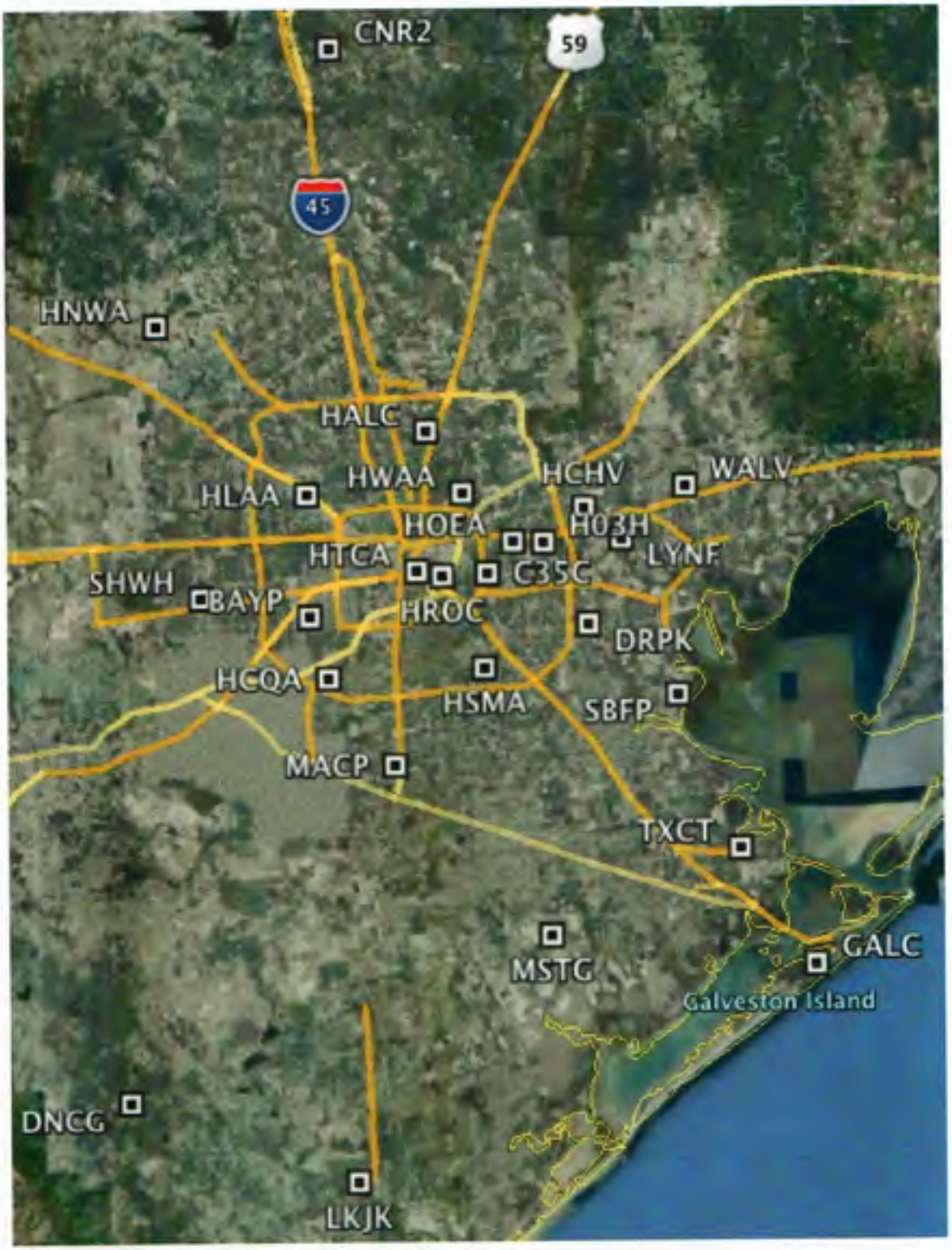

Figure 2.3: Map of Southeast Texas with monitors used in the TCEQ attainment demonstration (TCEQ, 2009a). Abbreviations are defined in Table 2.2

2.3 Process Analysis

Photochemical grid modeling data files provided for this study by the TCEQ and UH only recorded the spatial and temporal distribution of O_3 and its precursors. Rates of individual physical and chemical processes, which lead to the concentration changes in these species were not provided. With only concentration profiles, it becomes difficult to explain why air pollutant concentrations fields vary between specific days. Thus, having a more comprehensive assessment of all processes enables an improved understanding of the formation processes for pollutants. A complete assessment of the formation of O_3 and its precursors requires model diagnostic outputs. One type of such output is produced through an advanced probing tool called process analysis (PA). When the PA option is enabled in both models (CAMx and CMAQ) process rate data are recorded in two files, the Integrated Process Rate (IPR) and Integrated Reaction Rate (IRR). The IPR file contains physical process data for specified species for every time step at each grid cell for all layers. The process rates include advection, diffusion, deposition, and net chemistry. The IRR file contains data detailing the mass throughput of every reaction in the model's chemical mechanism.

These IPR and IRR files have data from every grid cell in the modeling domain resulting in confounding amounts of data. These data alone are not especially helpful and analysis larger than a grid cell is usually required. Therefore, a tool to sum processes across grid cells is required. A post-processing tool developed at UNC-CH, named pyPA (Python based Process Analysis) has the capability to aggregate each process rate over multiple grid cells and permits a thorough investigation of how the model reached its prediction. The pyPA tool can aggregate any area or collection of cells, known as a PA volume, and that shape can change vertically or horizontally as a function of time This methodology is described in detail by Kimura et al., 2007 and

Henderson, 2008.

The first step in producing PA output is to define the analysis area for the aggregation of process rates. This analysis region, labeled as the PA volume, can cover a number of horizontal and vertical grid cells. The horizontal domain of the PA volume used in this study is shown in Figure 2.4, and is made up of an area of 1,250 km^2 (6 x 13 4-km grid cells) encompassing both the Houston Ship Channel and downtown Houston. It was designed in this analysis to cover the most photochemically active region in the modeling domain. Hence, the calculated process rates are representative of the region and are not influenced by "hot emission" cells or non-typical inputs. This region is labeled as Central Houston (CHOU) and does not change horizontally with time. Vertically, however, the PA volume follows the hourly progression of a simulated PBL.

The PA volume is aggregated vertically to follow the simulated PBL, or the Model Mixing Volume (MMV). The MMV is determined by pyPA and is calculated differently depending on whether the model is CAMx or CMAQ. This is because each modeling system simulates the PBL differently. In CAMx, a meteorological post-processor, named MM5CAMx, calculates a vertical layer interface diffusivity or "k_v" (ENVIRON, 2005) to determine the extent of vertical mixing. The post processor calculates k_v parameters based on predictions of wind, temperature, and PBL parameters, generated by the PSU/NCAR mesoscale model (MM5) (Grell et al., 1995). The magnitude of the k_v parameter determines the amount of vertical transport from layer to layer and thus is used to obtain the MMV. To calculate a MMV from k_v values, ENVIRON developed a support tool VERTAVG that contains a direct quantitative relationship between k_v and MMV. At every grid cell, the algorithm goes layer by layer comparing the current cell's k_v with a "critical" k_v value ($k_{v,crit}$). The $k_{v,crit}$ is

Figure 2.4: The CHOU windowed 4-km domain including the ship channel, with 4 x 4 km grid and the Lambert Conformal Conical coordinates along the border. The process analysis volume (CHOU) is enclosed by the red box. The analysis volume has an area of 1,250 km^2 (6 x 13 4-km grid cells) incorporating both the Houston Ship Channel and downtown Houston. The brown and tan lines are the local highway system and blue is the Galveston bay and the Houston ship channel. Green squares represent ground monitors.

shown in Eq. 2.1,

$$k_{v,crit} = \frac{0.03[d_{z0}(d_{z0} + d_{z1})]}{200} \tag{2.1}$$

where d_{z0} is the thickness of the layer below the current layer, d_{z1} is the thickness of the current layer.

The algorithm goes through every cell vertically until it finds a k_v value that is lower than $k_{v,crit}$ meaning a lack of sufficient vertical transport to the next layer. The algorithm then defines that layer to be the top for the MMV. Based on these values, a MMV was chosen for every grid at every hour in the PA volume.

Unlike the CAMx system, in which the vertical diffusivity (k_v) were estimated in the meteorological post-processor, the CMAQ system explicitly predicts a PBL height, which is then used to determine the extent of vertical mixing. The explicit PBL height is generated by processing the MM5 mesoscale model data through a meteorology-chemistry interface processor (MCIP) that handles manipulation of meteorological input on different grids through simple bilinear interpolation (Byun and Ching, 1999). Depending on the user options, MCIP either directly passes through the surface and PBL parameters simulated by the meteorological model, or diagnoses them using the mean wind, temperature, and humidity profiles, surface data, and detailed landuse information available.

In this study, the former option is used. Thus, these quantities vary in space and time because of the varying terrain and atmospheric conditions. For the PA volume used in the CMAQ evaluations the top of the CHOU domain or MMV height was set equal to the explicit PBL reported by CMAQ.

Figure 2.5 shows the evolution of MMV for the CHOU domain. Included in the top graph are the domain wide average and the grid cell value of the maximum and minimum MMV for each hour. Excluded from this analysis were grid cells over water, as the MMV dynamics over these cells are very different. The bottom graphs display change in the spatial MMV in meters at 7 am and at 9 am for the CHOU domain while the rest of the 4 km domain is zero.

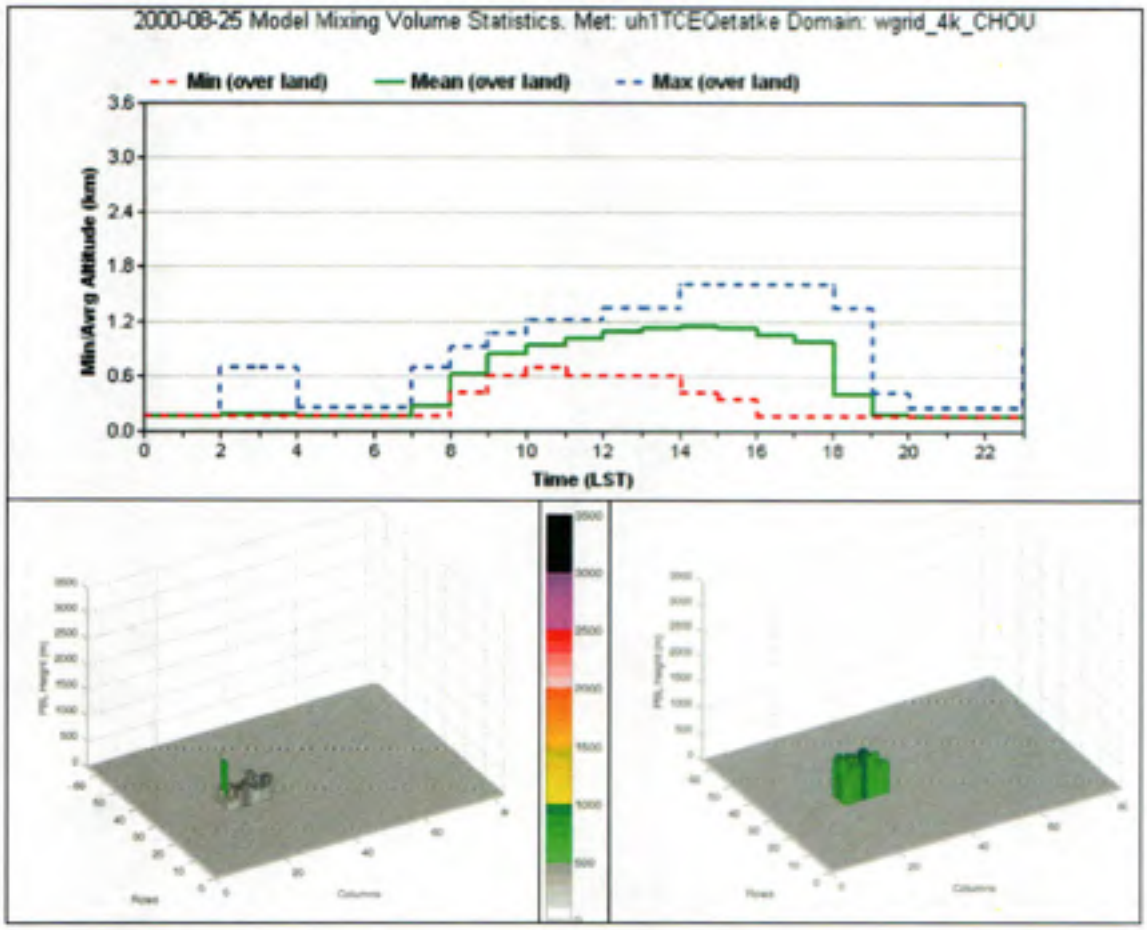

Figure 2.5: Evolution of Model MIxing Volume (MMV) for the Central Houston (CHOU) domain. (Top) The domain wide average and the grid cell value of the maximum and minimum MMV for each hour. Excluded from this analysis were grid cells over water, as the MMV dynamics over these cells are very different. (Bottom) The spatial MMV in meters per hour at 7 am and at 9 am for the CHOU domain.

CHAPTER 3

RESULTS

The following section describes the results of our model evaluation of O_3 predictions used in the HGB SIP for RRF_m calculations. The RRF_m metric is an average of O_3 predictions taken from multiple modeling days across the 2005, 2006, and 2018 modeling data set. Our analysis of these days show that many average RRF_m values use both weekend and weekday O_3 predictions made under different emission environments. In addition, an analysis of morning PBL rise showed two distinct types of phenomena that both produce high O_3, but one type is under a NO_x-limited condition and the other type is under a NO_x-inhibited environment. Thus, the response to emissions controls are different depending on the regime. The following sections present our finding from our analysis of day-of-week and morning PBL rise effects on O_3 production. Throughout the analysis, PA is relied upon to quantify the change in physical and chemical processes that lead to differences in O_3 production.

3.1 Weekday-Weekend Analysis

As described in the methodology section, we focused our analysis on the CHOU, including the ship channel and the main 610 highway loop, as shown in figure 2.4. In this region, it is expected that VOC, CO, and NO_x emissions would show daily variability due to human activity patterns. These changes in precursors concentrations can ultimately affect O_3 production. The temporal profiles of NO_x emissions are also different in the model. Figure 3.1, shows the NO_x emission rates in the CHOU region for June 21 and Aug. 6. It includes the mean NO_x emission rates, as well as the maximum and minimum rates found in the CHOU domain. The figure clearly shows

that weekend and weekday NO_x emission rates have different temporal patterns. Two peaks are observed in June 21 at morning and evening rush hour times of 2.4 and 2.8 x 10^8 moles/hr, while Aug 6 has only one peak at around noon of 1.8 x 10^8 moles/hr. Overall, the NO_x emissions are lower in the weekend. Our analysis of the 2000, 2005, and 2006 base case emission inventories show differences from day-of-week emission of VOC, CO, and NO_x; see Figure 3.2. This figure shows average daily concentrations for TCEQ's 2000, 2005, and 2006 for the designated CHOU domain. These emission rates are calculated by averaging the daily emission rates for all weekdays and again for only weekend days across all episode days. As shown in Figure 3.2, the percent reduction from weekday to weekend across all three simulations range from 11-13% for CO and 12-21% for NO_x. The largest difference in day-of-week emissions of NO_x (21%) occur in 2000, and the difference decrease in 2005 and 2006 simulations. This is because mobile emissions are a much larger fraction of the NO_x budget in the 2000 emission inventory than in the base case 2005 and 2006 emission inventories. Although the differences in weekend to weekday NO_x has decreased in the 2005 and 2006 base case EIs, they are still significant, 13%. In addition, changes in weekend-to-weekday VOCs have increased from 8% to 13% since the 2000 episode. These data suggest significant differences in emission rates due to the day-of-the-week.

Figure 3.3 shows the VOC/NOx, HRVOC/NOx and CO/NOx ratios calculated by averaging the daily emission rates for all weekdays and again for only weekend days. In the TCEQ 2000 episode, the VOC/NOx ratio increased by 16%, and the CO/NOx ratio increased by 12% due to large reductions in NO_x emissions. Although VOC and CO emission also were reduced, NO_x emission reductions were nearly double in magnitude. The HRVOC/NOx ratio increased by 24% due to HRVOC emissions remaining constant between weekends and weekdays. This consistency in HRVOC emissions could be due to industrial sources that operate continually throughout the

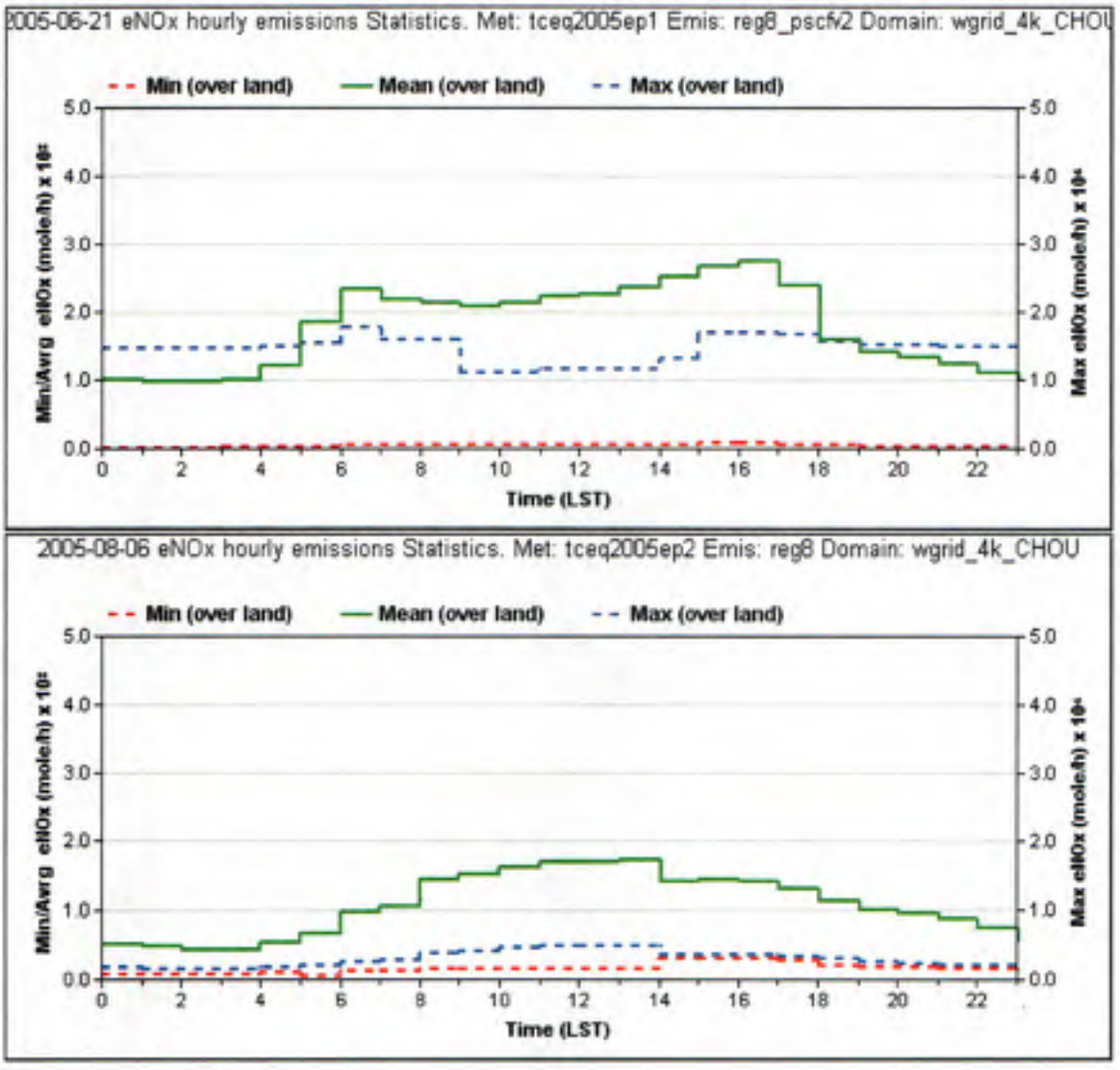

Figure 3.1: NO_xEmission Statistic for the weekday emission inventory (EI) (top) 06/21/05 and the weekend EI (bottom) 08/06/05 over the CHOU domain and simulated Planetary Boundary Layer (PBL). Included in the graph is the domain wide average and the maximum and minimum Model Mixing Volume (MMV) for a single grid cell at each hour. These emissions also include elevated sources. Excluded from this analysis were grid cells that had a land use described as water, as the MMV dynamics over these cells are very different.

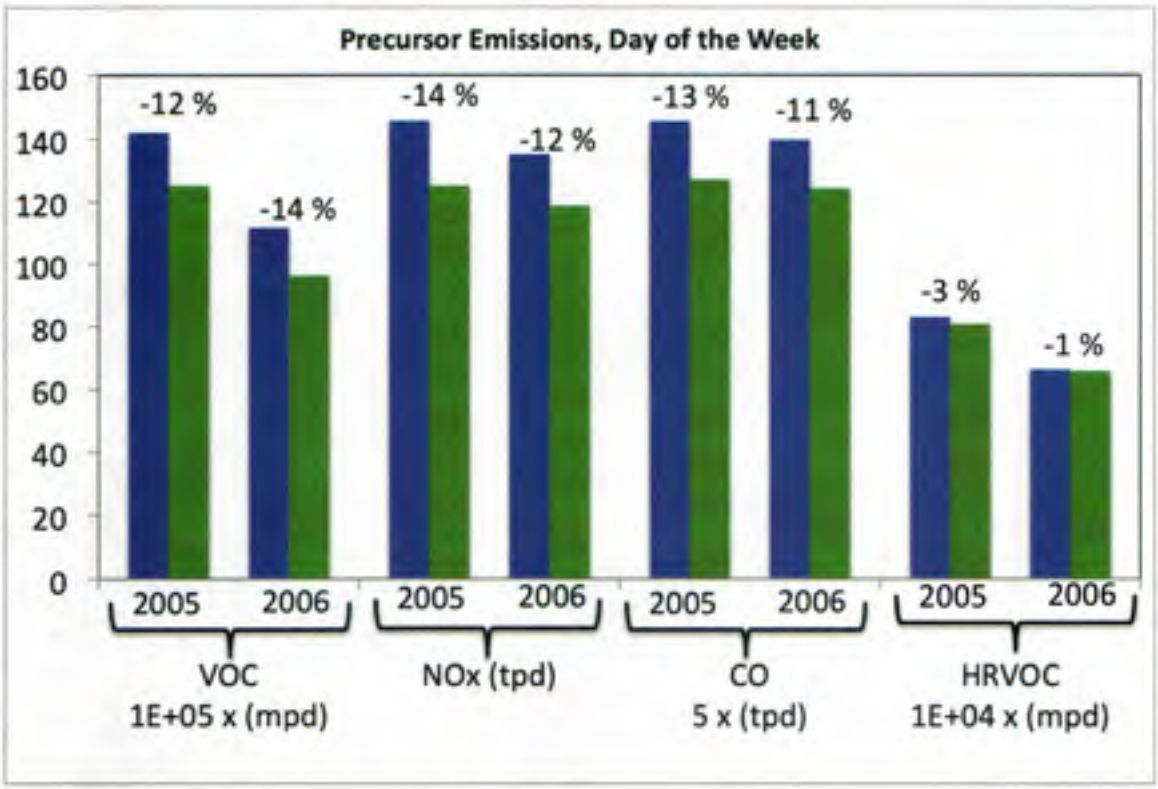

Figure 3.2: Weekday and weekend VOC, NO_x, and CO Emission rates for the 2000, 2005, and 2006 base case emission inventories for the CHOU domain. These emission rates are calculated by averaging the daily emission rates for all weekdays and again for only weekend days across all episode days.

entire week. The day-of-week differences for these ratios are smaller in the 2005 and 2006 episodes. In 2005, the VOC/NOx ratio difference is 2%, and in 2006 there is actually a 2% reduction from weekday to weekend. The CO/NOx ratio are nearly identical for all days in these episodes. There still persists a nearly 13% higher value for HRVOC/NOx ratios on weekends. In summary, the differences in weekday and weekend values for these precursor ratios have declined since the 2000 episode. This is mainly due to effective control strategies. The largest day-of-week differences were found in the HRVOC/NOx ratios.

The influence of day-of-week emission rates on O_3 was analyzed using predictions from the base line emission inventory used in the RRF_{2005} calculation. For RRF_{2005}

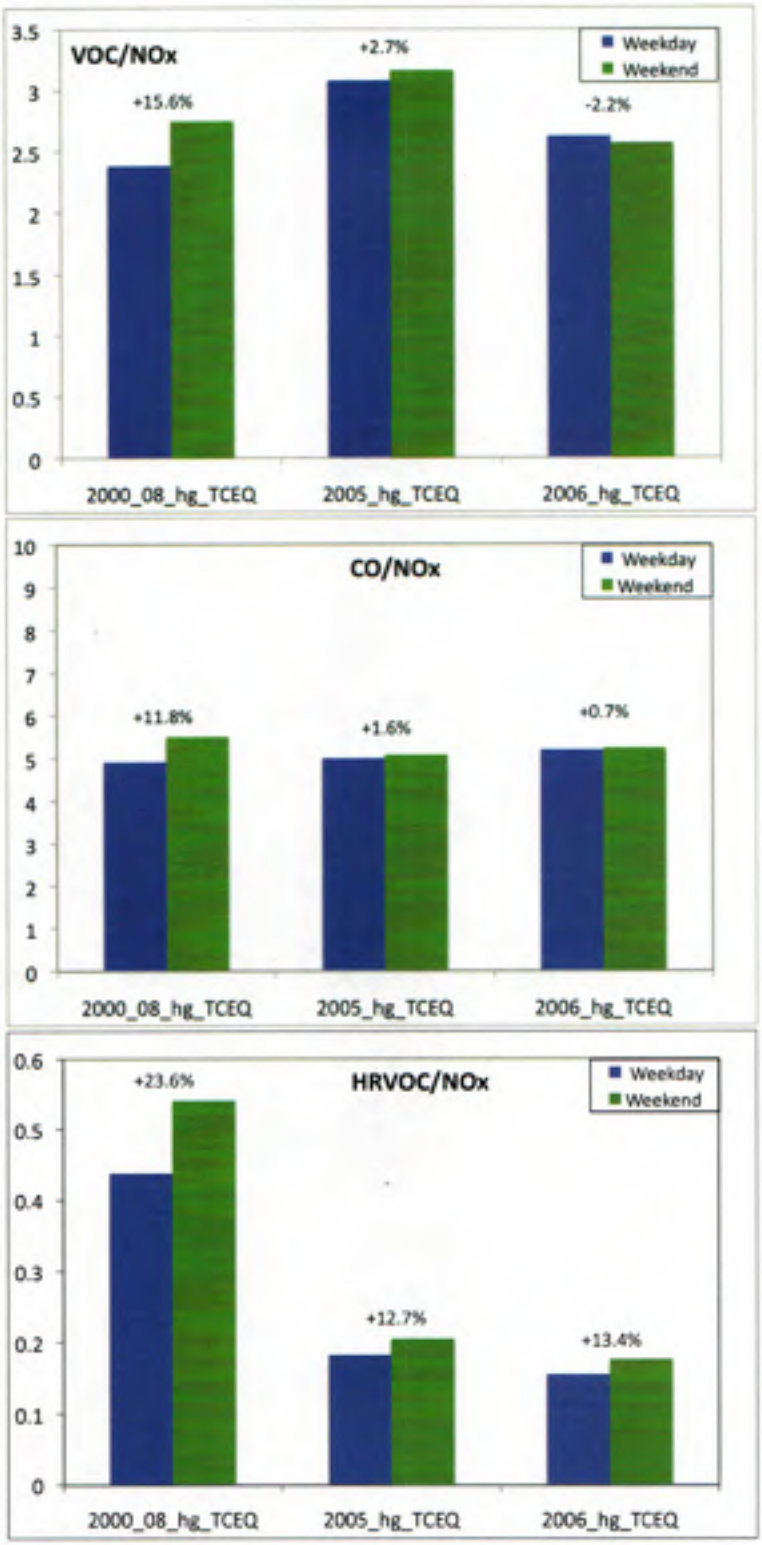

Figure 3.3: Weekdays and weekend VOC/NOx, CO/NOx and HRVOC/NOx for TCEQ base case 2000, 2005, and 2006 for the CHOU domain. Precursor ratios are calculated by averaging the daily emission rates for all weekdays and again for only weekend days.

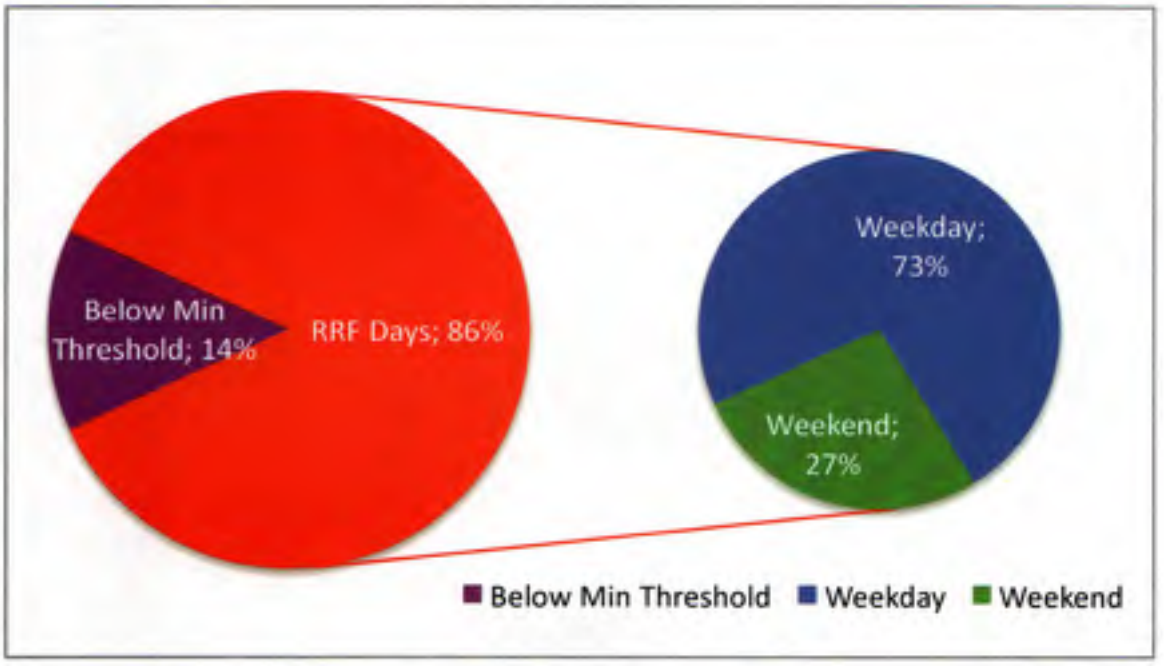

Figure 3.4: The total number of available modeling days and the fraction (red) used in the RRF_{2005} calculation. The distribution of weekdays (blue) and weekends (green) for these days are also shown.

calculations, 8-hr daily max O_3 concentrations are extracted from the model at a grid cell "near" a monitor location. This resulted in daily max O_3 concentrations from 73 modeled days in the 2005 and 2006 simulations. Only 63 days were actually used, since these complied with the minimum threshold of 85 ppb for daily 8-hr modeled maxima. The number of modeling days used to calculate a RRF_{2005} ranged from 9 days to 35 days, as shown in Table 3.1. Figure 3.4 shows the RRF_{2005} day distribution for day-of-the-week incidents for all days. Of the 63 days chosen for RRF_{2005} calculations, 46 days are weekend and 17 are weekends. The distribution for each monitor, however, is different. Percentages of weekends per monitor may range between 14-40%, imposing noteworthy weight when calculating RRF_{2005}s depending on the monitor, as shown in Table 3.1.

Table 3.1: The relative reduction factor calculated using all modeling days (RRF_{2005}), and using either weekend ($RRF_{2005,WE}$) or weekday ($RRF_{2005,WD}$) modeling days. The number of modeling days used for each monitor's RRF_{2005} are also shown. Monitors are geographically divided into monitors that are (top) less than and (bottom) greater than 25 km from downtown Houston.

Site	$RRF_{2005,WD}$		$RRF_{2005,WE}$		RRF_{2005}	
	Days	Value	Days	Value	Days	Value
SHWH	22	0.848	8	0.816	30	0.840
BAYP	24	0.876	9	0.822	33	0.861
HLAA	23	0.864	7	0.836	30	0.857
HCQA	24	0.869	8	0.815	32	0.856
HTCA	22	0.921	4	0.848	26	0.910
HALC	17	0.889	5	0.864	22	0.883
HROC	21	0.931	4	0.860	25	0.919
HWAA	18	0.907	3	0.880	21	0.902
HSMA	26	0.902	9	0.871	35	0.894
C35C	21	0.935	6	0.891	27	0.925
HOEA	19	0.926	6	0.904	25	0.922
H03H	20	0.936	5	0.923	25	0.934
DRPK	19	0.920	8	0.921	27	0.922
HCHV	17	0.941	4	0.931	21	0.939
LYNF	17	0.950	4	0.935	21	0.947
SBFP	14	0.916	5	0.927	19	0.919
WALV	12	0.923	3	0.936	15	0.925
DNCG	6	0.855	3	0.843	9	0.851
HNWA	17	0.839	4	0.853	21	0.842
LKJK	8	0.867	4	0.888	12	0.872
CNR2	6	0.862	4	0.844	10	0.855
MACP	25	0.868	8	0.859	33	0.866
MSTG	11	0.877	3	0.876	14	0.877
TXCT	15	0.916	6	0.924	21	0.918
GALC	17	0.920	3	0.928	20	0.922

Figure 3.5 shows the S_{2005}, or "qualified" maximum 8-hr predicted base line case ozone "near" a monitor, in a box and whisker plot, where each day was divided into weekday (blue) and weekend (green). The box and whisker plot extends from the lower to upper quartile values of the data, with a line at the median. Outlier points are those past the end of the whiskers and are only displayed if data point

exsist outside upper and lower quartiles. The monitors are organized from West to East. The monitors are organized from West to East and segregated geographically where the monitors in the left panel are within 25 km of downtown Houston. The monitors are divided into this set because the production for O_3 is different outside the heavy urban area of Houston and the less urban areas farther from downtown. The geographic distribution of monitors is shown in Fig. 2.3.

As shown in Figure 3.5, monitors located in the eastern region of Houston (WALV, LYNF and HCHV) had O_3 predictions that were higher on weekends than on weekdays. Even though SBFP is farther to the East, the monitor is located farther South than HCHV, LYNF, and WALV. Thus, it is not strongly influenced by the same emissions as these eastern monitors. As a result, there is a negligible change between the S_{2005} medians between weekend and weekdays. At the rest of monitors, however, the predicted weekend O_3 rarely surpasses that of weekdays. The predicted O_3 concentrations in the West are just the opposite. At the SHWH, BAYP, and HLAA monitors O_3 is predicted higher on the the weekdays. At the remaining monitors in the urban core of Houston, there is very little difference in the weekday and weekend medians. The highest O_3 concentrations, however, are nearly always weekdays. These data suggest that responses in O_3 to changes in emissions due to day-of-week are dependent on the location of monitors.

Figure 3.6 shows $\overline{S_{2005}}$, or the average of "qualified" maximum 8-hr predicted base line case ozone "near" a monitor, for all monitors averaged for all modeling days (red), or averaged across modeling days that were either weekends (green) or weekdays (blue). Similar to Figure 3.5, the monitors are in geographic order from the western-most to eastern-most regions of Houston. In the western region of Houston, at monitors such as SHWH, BAYP, and HLAA, O_3 concentrations predicted more

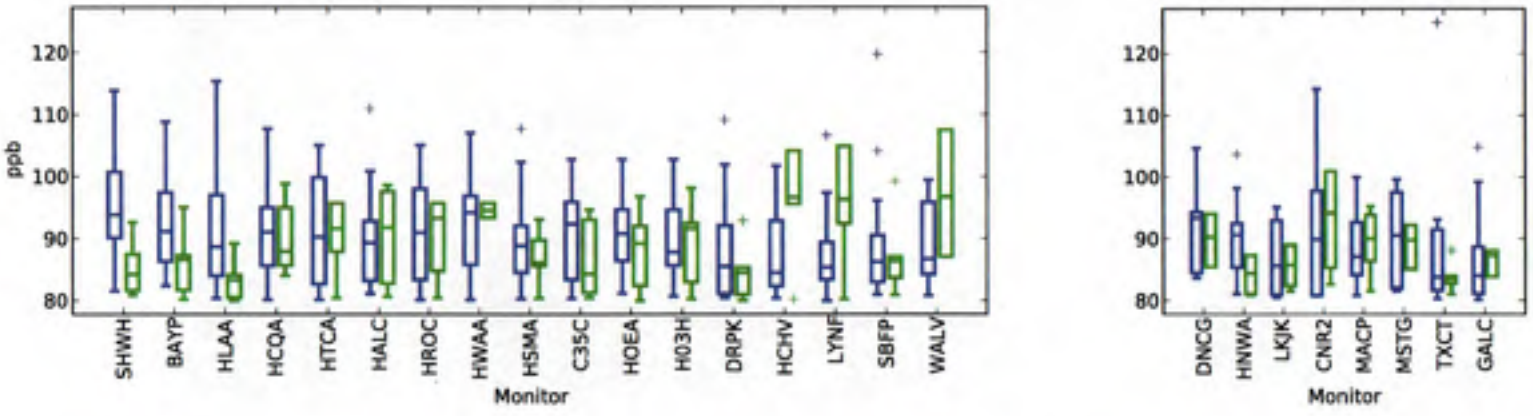

Figure 3.5: The box and whisker plot of the average of max 8-hr modeled concentrations for the base line case simulations of 2005 and 2006. The plot extends from the lower to upper quartile values of the data, with a line at the median. Outlier points are those past the end of the whiskers and are only displayed if data point exsist outside upper and lower quartiles.This data is further classifies as weekday (blue) and weekend (green) for every monitor. Monitors are geographically divided into monitors that are (left) less than and (right) greater than 25 km from downtown Houston.

than a 10 ppb difference between weekday and weekend, with weekdays predicting the higher value. At the eastern monitors (HCHV, LYNF, and WALV) the models also predicted a large difference, ~7 ppb, in predicted O_3 between weekends and weekdays. The model tended to predict higher O_3 concentrations on weekdays in the West and on weekends in the East. The model predicted O_3 for the Houston urban core shows less of a difference between weekdays and weekends. Model predictions made at the HWAA monitor, however, did show a higher O_3 concentration on the weekend. At this monitor location, of the 21 modeling days used to calculate the $\overline{S_{2005}}$, only 3 were weekends biasing this value. O_3 predicted at monitors more than 25 km from downtown Houston were mostly less than 2 ppb, with the exception of HNWA with 6 ppb.

The $\overline{S_{2018,m}}$, or the average of "qualified" maximum 8-hr predicted future case ozone "near" a monitor, were also calculated and are shown in Figure 3.6. In comparison to $\overline{S_{2005}}$, the $\overline{S_{2018}}$ for all days show an average of a 10% reduction. In the 2018 episode, O_3 predictions at western monitors, from SHWH to HCQA show the largest reduction of ~15%. A smaller reduction was predicted in the East (HCHV, LYNF, and WALV), ~6%, and for all other monitor locations there was an average ~9% reduction. The model predicted a larger reduction in O_3 concentrations for weekend days than weekdays. For example, at the HCQA monitor the weekday average went down 13 ppb, and the weekend average was reduced 16 ppb. This suggests that weekend days are more responsive to future changes in the precursor emissions changes tested here. The predicted O_3 differences between weekend and weekday days in 2018 also show a geographic trend. In the Houston urban core (HCQA to HO3H) the difference is 2-9 ppb, 7-11 ppb at the western monitors SHWH, BAYP, HLAA, and HCQA, and in the East the HCHV, LYNF and WALV monitors a difference of 4-10 ppb. As with the 2005 base line simulation, in this model series the eastern

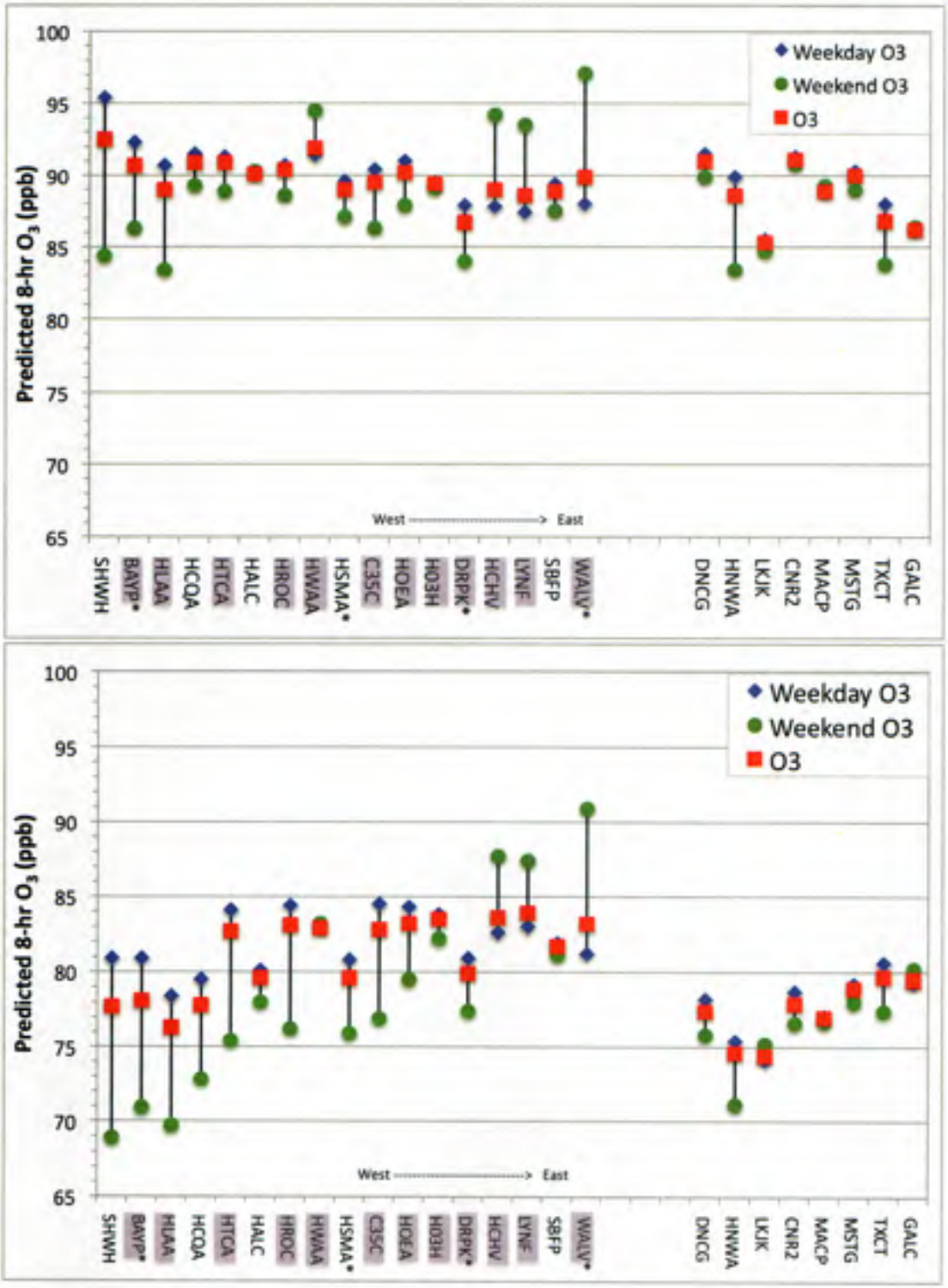

Figure 3.6: Base line episode (Top) and 2018 episode (Bottom) predicted daily max 8-hr modeled concentrations near a monitor averaged across all days (red), weekdays only (blue) and weekends only (green). Monitors are dived geographically between those monitors (left) less than and (right) more than 25 km from downtown Houston. Highlighted monitors are inside CHOU. Starred monitors failed TCEQ's attainment test.

monitors had a higher predicted O_3 concentration for weekend days, and the western monitors predicted higher O_3 on weekdays. At most of the monitors farther than 25 km from downtown Houston the model predicted a difference of less than 2 ppb. The exceptions were at the HNWA and TXCT monitors where the difference was as large as 6 ppb. The location of both these monitors may attest to the reason behind these outliers. TXCT is close to a small urban population and could be affected by mobile emissions. On observed high O_3 days at the HNWA monitor, back trajectories have shown impacts of emissions from the CHOU region as shown in appendix B.2. Thus, changes in mobile NO_x emissions due to day-of-week could also be affecting the model predictions at this monitor.

Figure 3.7 and Table 3.1 show the RRF_{2005} based on all qualified modeling days, and two surrogate RRF_{2005} s each based solely on weekday ($RRF_{2005,WD}$) or weekend ($RRF_{2005,WE}$) episode days. To calculate the $RRF_{2005,WD}$, the $\overline{S_{2018}}$ for weekdays is divided by the $\overline{S_{2005}}$ for weekdays. Since weekends are less frequent than weekdays the recommended minimum of 10 days was not enforced. From HOEA to WALV differences between $RRF_{2005,WD}$ and $RRF_{2005,WE}$ are 2%. Farther West the difference grows. From SHWH to C35C monitors the $RRF_{2005,WD}$ are 3% to 8% lower than $RRF_{2005,WE}$. In all three RRF_{2005}s there was a linear trend from West to East meaning that the western side of Houston is more responsive to these controls than the eastern side. Moreover, the relative reduction factors show that most weekends are more responsive to emission reductions than weekdays. Additionally, the monitors further than 25 km from downtown Houston depict the same increase in RRF_{2005} trend from West to East. The response difference between weekdays and weekends RRF_{2005} s is less than 2%.

The larger differences in RRF_{2005} introduces larger margins of uncertainty and may affect a monitor's reaching attainment. Figure 3.8 shows the DV_F for each monitor

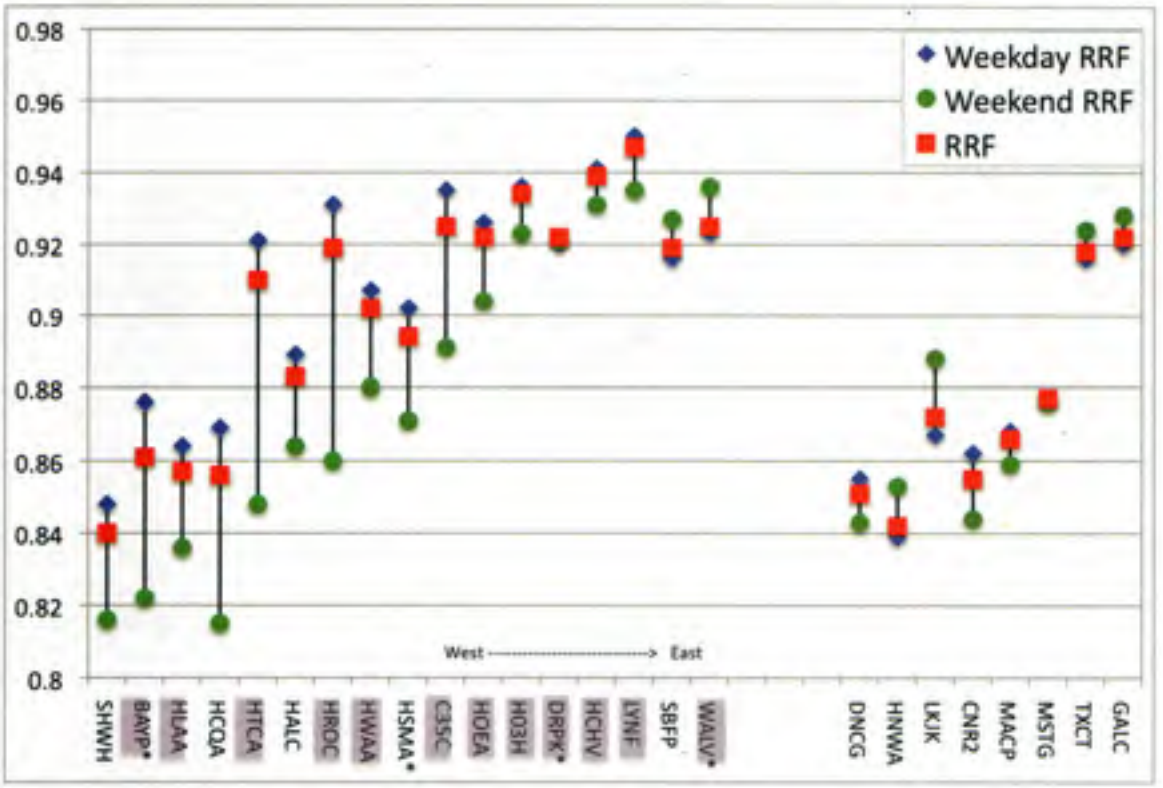

Figure 3.7: Relative reduction factor for all monitors calculated using all days (RRF_{2005}, red), and using onyly weekdays ($RRF_{2005,WD}$, blue) or only weekends ($RRF_{2005,WE}$, green). Monitors are ordered West to East and dived geographically between those monitors (left) less than and (right) more than 25 km from downtown Houston. Highlighted monitors are inside CHOU and starred monitors failed TCEQ's attainment test .

based on the SIP RRF_{2005} and surrogate $RRF_{2005,WD}$ and $RRF_{2005,WE}$. The range of the difference between weekday DV_Fs and weekend DV_Fs is 2-6 ppb in the western side of CHOU from SHWH to HOEA where weekends have a lower DV_F. Less than ~1 ppb difference between weekdays and weekends is predicted in all other monitor locations. This suggests the $DV_{B,2005}$ has a larger influence than the response by the model. Given that DV_Fs should be below 85 ppb to achieve attainment, four monitors are considered out of attainment, BAYP, HSMA, DRPK, and WALV. The DV_Fs for BAYP and HSMA, nonetheless, have weekend DV_Fs that are in attainment.

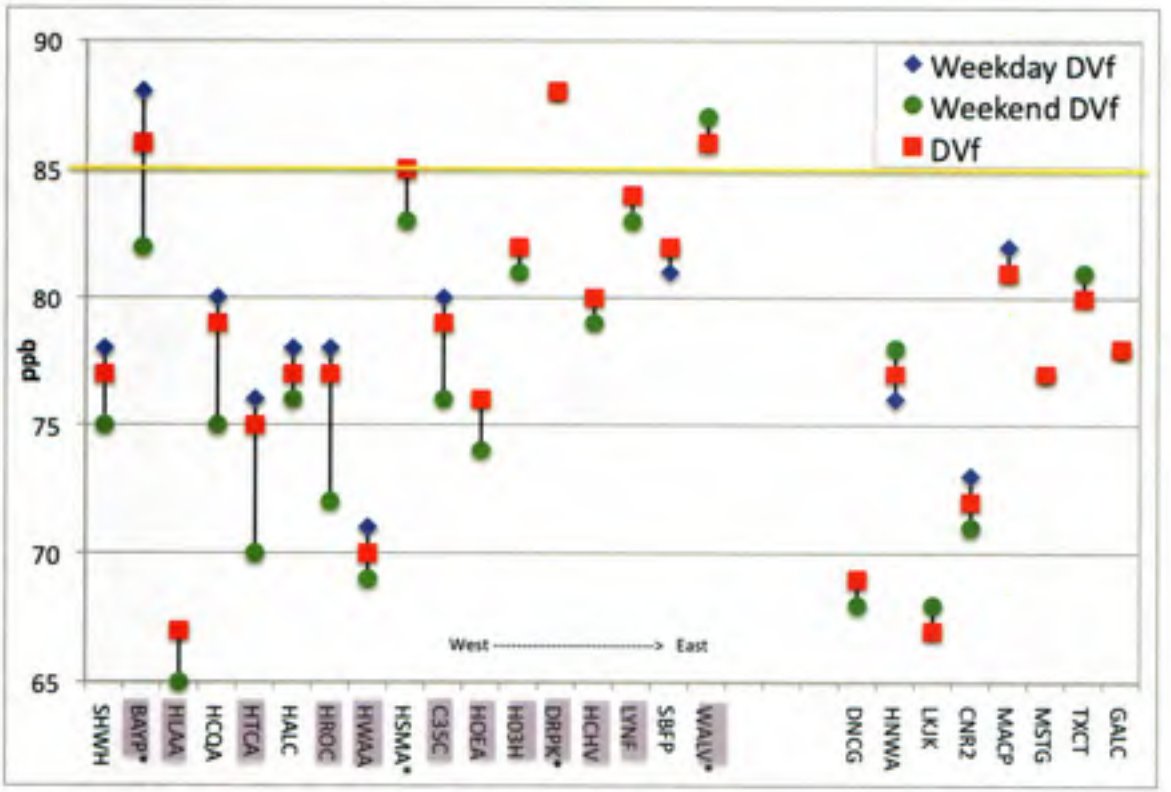

Figure 3.8: DV_F by monitor calculated using RRF_{2005} (red), $RRF_{2005,WD}$ (blue), and $RRF_{2005,WE}$ (green). Monitors are dived geographically between those monitors (left) less than and (right) more than 25 km from downtown Houston. Highlighted monitors are inside CHOU and starred monitors are in non-attainment.

In summary, western monitors demonstrated greater response to the simulated controls in 2018. These controls include a 78% reduction of mobile emissions. The western CHOU covers an area of heavy traffic and is dominated by mobile emissions. The industrial source dominated eastern CHOU, on the other hand, had a weaker response to controls in the 2018 simulation. Overall, reduction in the western monitors was almost twice that in the eastern monitors. When NO_x emissions were changed due to day-of-the-week, the effect on RRF_{2005} was less response on weekdays.

3.2 Meteorological Analysis Results

Meteorology influences the evolution of emissions and chemical species. Moreover, wind and vertical diffusivity inputs are the basis of vertical advection, dispersion, and diffusion calculation. One meteorological feature critical to air quality is the evolution of the PBL. The model's ability to replicate this feature and its effect on O_3 formation is the focus of this analysis. As described in the methodology we are able to calculate the simulated PBL, or MMV, for every grid cell in the domain. We analyzed MMV values for all modeling episodes listed in Table 2.1. We also focused our analysis on the CHOU region of the domain.

The result of this analysis showed either a "rapid" or "slow" rise in the morning MMV. A "rapid" rise we have defined as a MMV change of greater than 700 m/hr between the hours of 6-11 LST, and a "slow" rise we defined as a MMV change less than 700 m/hr. This classification was completed looking at the evolution of the MMV for the entire available dataset and choosing a demarcation, with the help of figures such as 3.9. These figures show the evolution of MMV in the CHOU domain. Included in these figures are the domain wide average and the grid cell value of the maximum and minimum MMV for each hour. Excluded from this analysis were grid cells that had a land use described as water, as the MMV dynamics over these cells are very different. Using these figures, changes in MMVs were observed that range up to 1100 m/hr.

An example of a slow riser is shown in Figure 3.9. This episode showed that between the hours of 7 -13 LST the MMV rises between 200 to 400 m/h. There is a constant 200 m mean MMV from 0 to 8 LST. This constant value is usually set by the meteorological model parameters and is not physically real. Later in the day, a stepwise increase is observed at the start of the photochemical day in both domains.

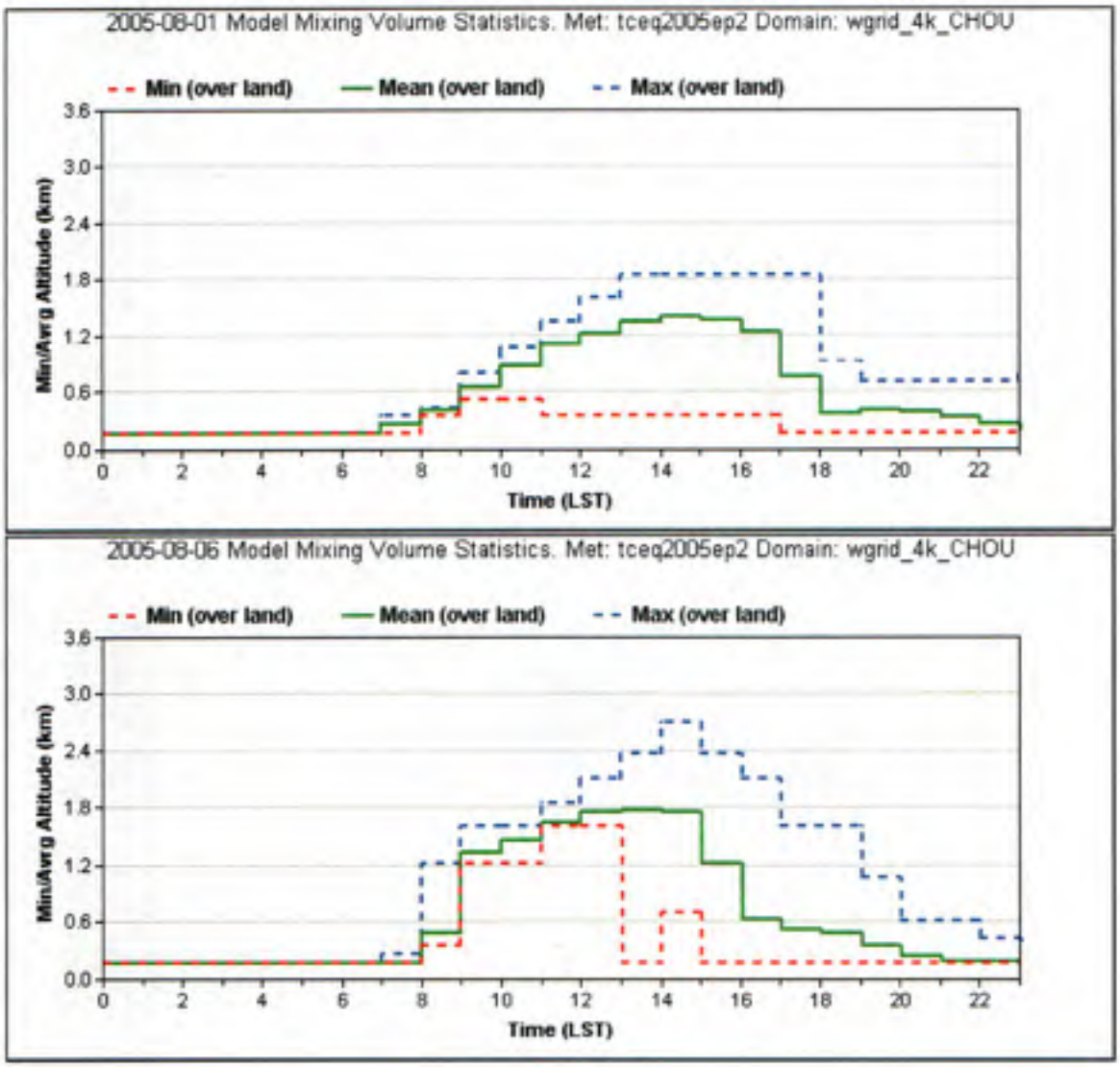

Figure 3.9: 08/01/05 "Slow Riser" (Top) and 08/06/05 "Fast Riser" (Bottom) MMV Statistic for the CHOU Domain. Included in the graph are the domain wide average and the maximum and minimum MMV for a single grid cell at each hour. Excluded from this analysis were grid cells that had a land use described as water, as the MMV dynamics over these cells are very different.

In addition during hours 8-11 LST the minimum and maximum values are close to the average value. This means that the entire CHOU domain showed similar increases in MMV. The MMV mean peak is ~1400 m at around 14 LST. After hour 14 LST, the MMV begins to drop.

An example of a rapid morning rise MMV is shown in Figure 3.9. On this day, the MMV shows a mean morning rise at 9 LST of ~850 m/h. From hours 0 to 6 LST the mean MMV between the slow riser and the fast riser are very similar. After the start of the photochemical day, 8-9 LST, MMV behaviors differ. The fast risers MMV shows increases in the morning of more than 700 m/hr. The MMV mean peak is ~1800 m at around 14 LST. After this time, the MMV begins to drop. By 16 LST ~66% of the mean MMV has dropped from the peak. It is also important to note that during hours 7-12 LST that the minimum, maximum, and mean MMV in the CHOU domain are very close in the fast riser. The slow riser, on the other hand, minimum begins to differ that of the mean by 10 LST. The hours were the minimum and maximum follow the mean closely suggest that the entire CHOU domain is experiencing similar rises in MMV.

Differences in the type of MMV riser were also analyzed spatially across the domain. A windowed 4-km grid domain for the 2 types of risers is shown in Figure 3.10 and shows the hourly MMV value and average wind vector for every grid scale. At 7 LST none of the cells shows a peak above 600 m (Refer to appendix C.1). At hour 9 LST, however, the spatial plots depict very different MMV heights. At this time, two-thirds of the cells in the 4-km windowed domain for the slow riser are barely reaching 600 m. The cells in the fast riser, on the other hand, attain MMV heights of 1800 m. Moreover, the fast riser at this time has MMV heights that the slow riser does not get to all day. Recalling the time series plots of these days (Figure 3.9), it is observed that both risers reach MMV peaks around the same time around 14 LST, but the max mean MMVs differ by more than 400 m. Although these days had different meteorologies, each had 1-hour peak O_3 higher than 100 ppb (08/01/05 with ~145 ppb and 08/06/05 with ~103 ppb) and are relevant to the SIP. These results imply that in very different meteorological conditions, high amount of 1-hr modeled

O_3 is predicted.

For the remainder of this analysis we will classify modeling episode days based on the fast and slow rise criteria stated above, but only for the CHOU domain. The greater part of the days of the 2000 TCEQ episode shows behavior of a slow riser. This is attributed to the PBL nudging by the TCEQ on this episode (TCEQ 2009b). The nudging of the PBL was deemed necessary, because the preliminary model (MM5) lacked the ability to produce proper vertical mixing estimations for the area (Nielsen-Gammon 2002). Simulations of the base case 2005 and 2006 episodes also show this slow riser behavior. For instance Figure 3.11 shows that June 21, 2005 and August 17, 2006 were classified as slow rising days because both days had morning MMV rises of less than 700 m/hr. Another similarity in both days is that the maximum and minimum MMVs diverge quickly by hour 12 LST. Additionally, June 21 and Aug. 17 are high O_3 days with 1-hour O_3 peaks of 101 and 132 ppb, and are used in the RRF_{2005} calculation for the attainment demonstration. One main difference between these days is that June 21 reaches MMVs peaks of more than ~1800 m while Aug 17 shows peaks no higher than ~1700 m.

Rapid morning rise MMV behavior was not seen in the 2000 episode, but were present in the 2005 and 2006 episodes. A number of days in 2005 and 2006 episodes predicted fast rising behavior. High O_3 days such as September 1, 2006 and June 19, 2005 portray this trend, as shown in Figure 3.12. Sept. 1 and June 19 have high 1-hour O_3 peaks of 127 and 105 ppb, respectively. Although both days are classified as fast risers, there are still differences later in the day in the timing of the collapse of the MMV. From midnight until the peak MMV is reached at 13 LST, the average MMVs on both days were similar. These similarities end, however, after a significant MMV drop of ~1200 m by 18 LST on Sept. 1. The mean MMV for June

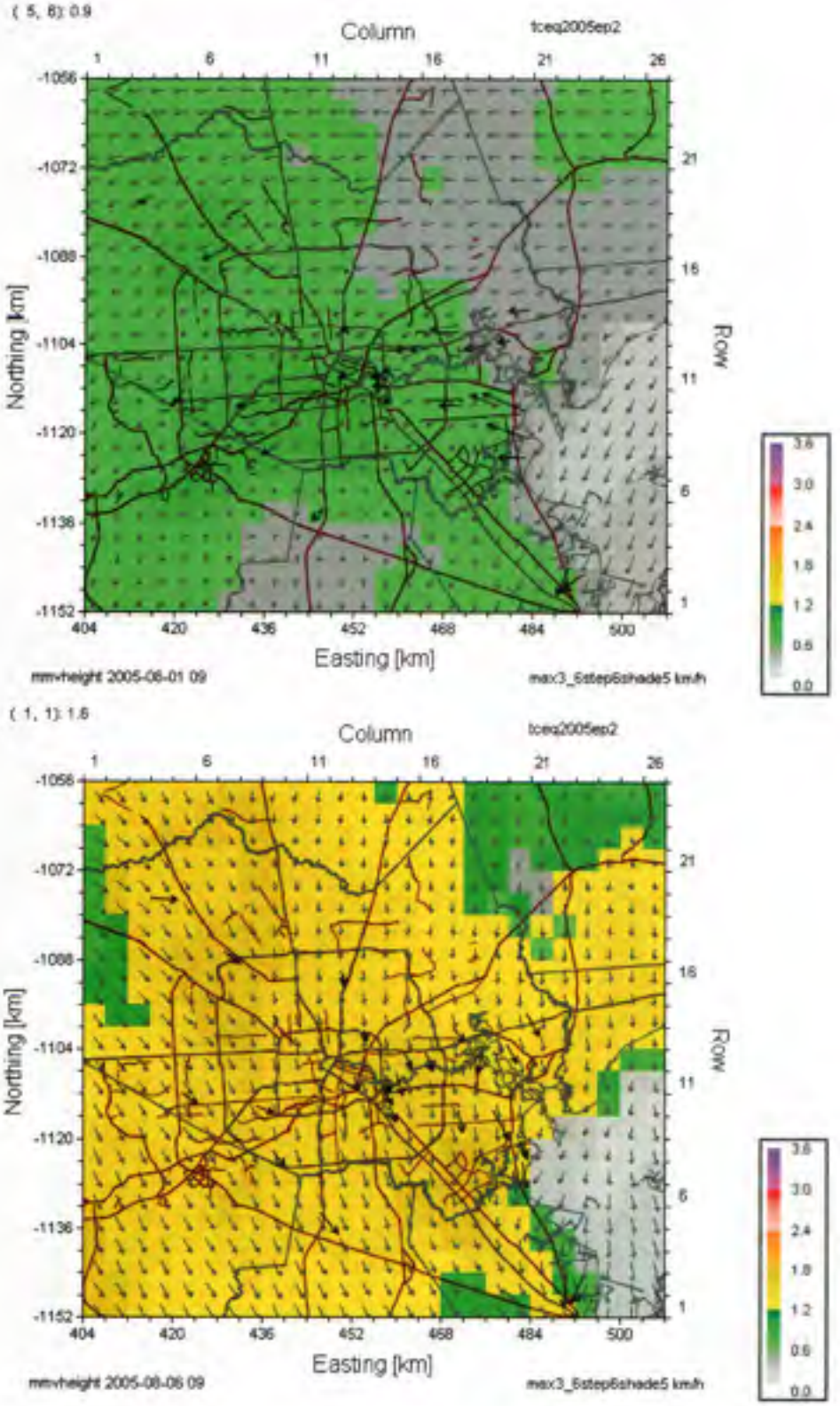

Figure 3.10: MMV height (km) Spatial Tile plot for the 4km windowed domain for slow riser (left) 08/01/05 and fast riser (right) 08/06/05 at 9 am. The tan and grey lines represent highway systems and major roads. The arrows represent hourly average wind direction.

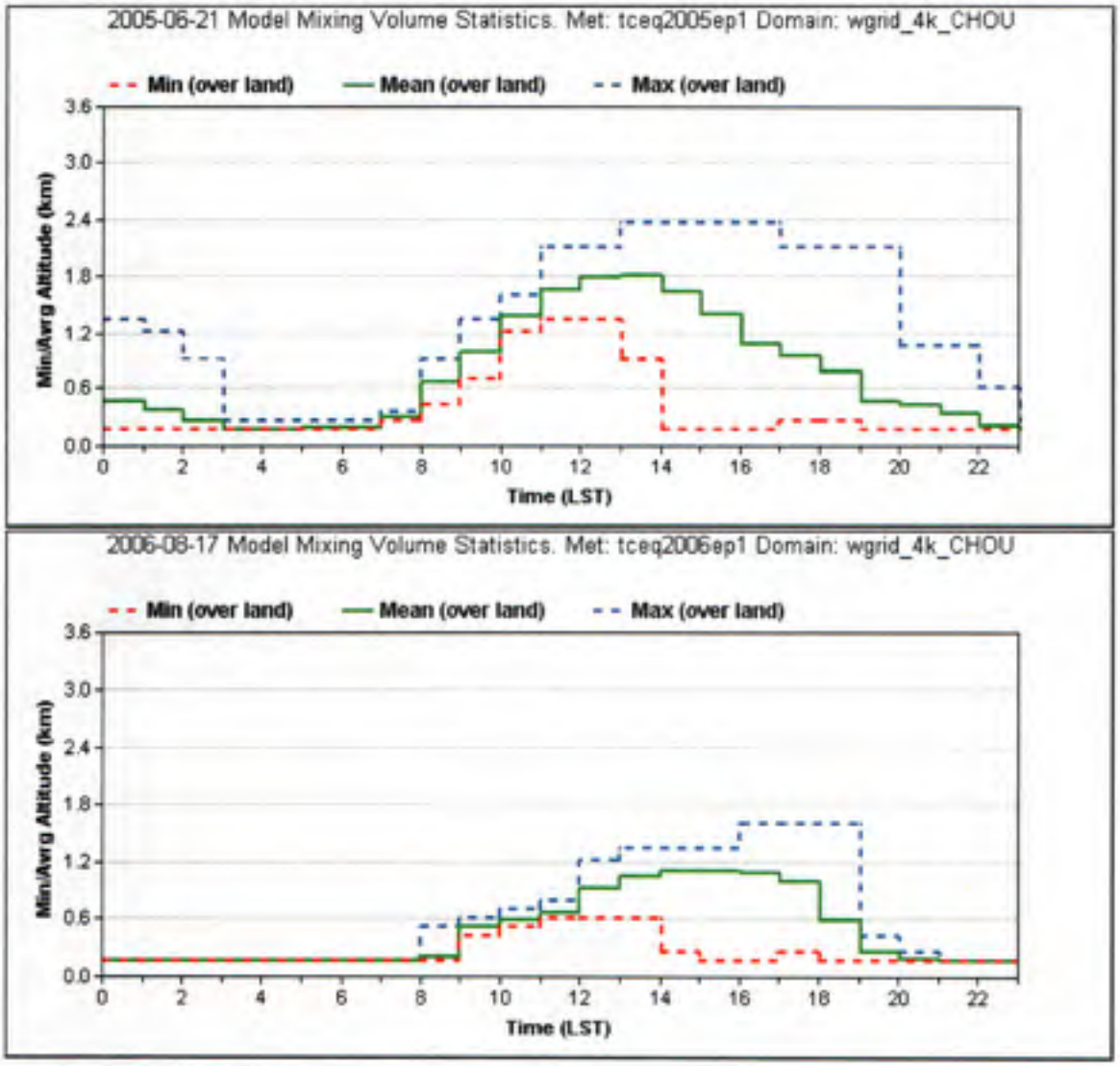

Figure 3.11: Slow riser MMV Statistic for (Top) 06/21/05 and (Bottom) 08/17/06 for the CHOU domain. Included in the graph is the domain wide average and the maximum and minimum MMV for a single grid cell at each hour. Excluded from this analysis were grid cells that had a land use described as water, as the MMV dynamics over these cells are very different.

19 reaches this height by 20 LST. The maximum MMV heights are also quite different in both models. June 19 has a max MMV that fluctuates even before dawn. This is phenomena is seen in other episode days and requires further investigation outside the scope of this report. Another difference between these fast risers is that June 19 does not fully decrease until after 21 LST. Meanwhile, Sept. 1 maximum MMV not

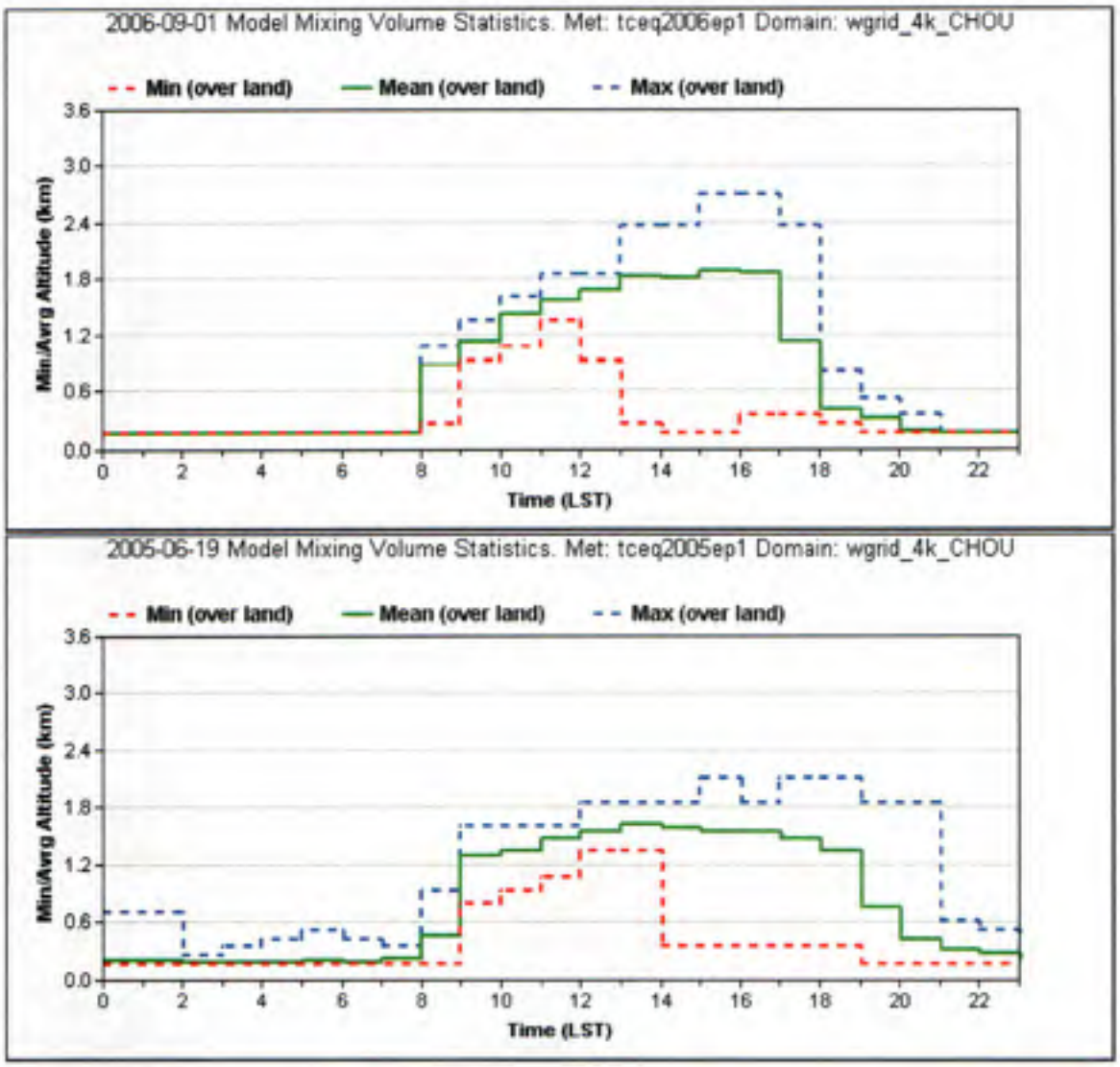

Figure 3.12: Fast riser MMV Statistic for (Top) 09/01/06 and (Bottom) 06/19/05 for the CHOU domain. Included in the graph is the domain wide average and the maximum and minimum MMV for a single grid cell at each hour. Excluded from this analysis were grid cells that had a land use described as water, as the MMV dynamics over these cells are very different.

only reaches a peak above ~2400 m, but begins its decrease earlier at 15 LST.

Of the 63 RRF_{2005} modeling days from the 2005 and 2006 TCEQ episodes, 22 days contain fast risers and 41 slow risers, as shown in Figure 3.13. The percentages of fast risers per monitor may range between 58% and 20%. Table 3.2 shows the

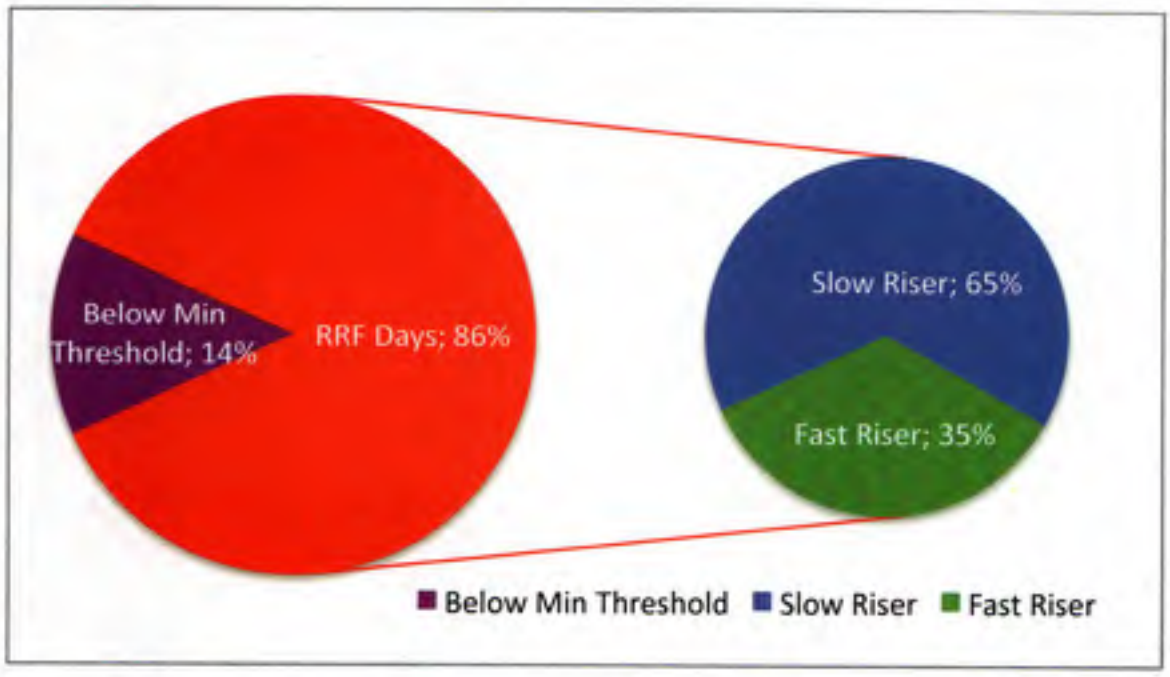

Figure 3.13: RRF_{2005} days distribution for all available days and the distribution of slow riser (blue) and fast riser (green).

distribution between RRF_{2005} modeling days for each type of morning MMV rise for each monitor. Overall, the fast rising phenomenon accounts for more than 20% of RRF_{2005} days used in calculations, imposing noteworthy weight when calculating the RRF_{2005}. Additionally, of the 17 weekends used in RRF_{2005} calculations, 11 are fast risers and of the 46 weekdays 11 are fast risers.

The rise of the MMV heights will affect pollutant concentrations, transport of pollutants, and the chemical kinetics of O_3 production. In addition, the differences of the timing and rate of the rise and fall of the MMV height will influence O_3 production because those times coincide with large emission of O_3 precursors. The impact on predicted O_3 concentrations was analyzed using the max 8-hour O_3 values used for the RRF_{2005} calculation. Figure 3.14 is a box and whisker plot of this data segregated by fast and slow riser days. As the figure shows, O_3 predictions in the fast riser days in East at the DRPK, HCHV, LYNF, and WALV monitors are higher than the

Table 3.2: Relative reduction factors calculated with all modeling days (RRF_{2005}), or solely with days classified as fast riser ($RRF_{2005,FR}$) or slow riser ($RRF_{2005,SR}$). Also shown are the number of days used in each calculation at every monitor. Monitors are ordered East to West and are further divided into monitors that are (top) less than or (bottom) greater than 25 km from downtown Houston.

Site	$RRF_{2005,SR}$		$RRF_{2005,FR}$		RRF_{2005}	
	Days	Value	Days	Value	Days	Value
SHWH	20	0.851	10	0.819	30	0.840
BAYP	21	0.878	12	0.833	33	0.861
HLAA	20	0.869	10	0.837	30	0.857
HCQA	21	0.870	11	0.829	32	0.856
HTCA	18	0.933	8	0.861	26	0.910
HALC	14	0.903	8	0.849	22	0.883
HROC	17	0.936	8	0.884	25	0.919
HWAA	14	0.914	7	0.881	21	0.902
HSMA	22	0.905	13	0.877	35	0.894
C35C	17	0.938	10	0.905	27	0.925
HOEA	15	0.936	10	0.903	25	0.922
H03H	16	0.942	9	0.917	25	0.934
DRPK	13	0.929	14	0.913	27	0.922
HCHV	12	0.958	9	0.913	21	0.939
LYNF	12	0.962	9	0.927	21	0.947
SBFP	8	0.930	11	0.910	19	0.919
WALV	9	0.936	6	0.911	15	0.925
DNCG	6	0.864	3	0.823	9	0.851
HNWA	14	0.843	7	0.836	21	0.842
LKJK	9	0.872	3	0.877	12	0.872
CNR2	8	0.864	2	0.824	10	0.855
MACP	20	0.881	13	0.839	33	0.866
MSTG	7	0.874	7	0.881	14	0.877
TXCT	9	0.920	12	0.917	21	0.918
GALC	9	0.922	11	0.921	20	0.922

predicted O_3 on slow riser days. In the west, however, O_3 predictions on fast riser days are lower than on slow riser days with the exception of BAYP, HTCA, HROC, and C35C monitors. No such geographic pattern was predicted at monitors that were more than 25 km from downtown Houston. These data suggest that the model response to morning MMV rise is dependent on whether you are on the West or East

side of Houston.

Figure 3.15 shows the $\overline{S_{2005}}$ across all RRF_{2005} days, and specifically across those days with slow or fast morning rises. The plot shows that in the West at the SHWH, BAYP, HLAA, and HCQA monitors the model predicted higher $\overline{S_{2005}}$ on slow riser days. In the East H03H, DRPK, HCHV, LYNF, and WALV, show that $\overline{S_{2005}}$ on fast riser days are an average of ~4 ppb higher than slow riser days. The Houston urban core has variable O_3 between fast risers and slow risers. Most of the monitors do not show, however, differences between risers of more than 2 ppb. The monitors more than 25 km from downtown Houston do not show this trend. Figure 3.15 also shows the $\overline{S_{2018}}$ across all days, and just for fast or slow riser days. In 2018, model predictions West of the HROC monitor, on slow riser days, had the largest reductions in O_3 of up to 6-8 ppb. Predicted reductions from east of the HROC monitor, were less with differences of ~2 ppb.

Figure 3.16 and Table 3.2 display the RRF_{2005} calculated for the TCEQ SIP that uses all episode days. Also shown is a new RRF_{2005} based on using only slow riser days ($RRF_{2005,SR}$) and only fast riser days ($RRF_{2005,FR}$). As seen previously, the RRF_{2005} increase from West to East showing that the most responsive areas are in the western side of Houston. At every monitor the $RRF_{2005,FR}$ had lower values than the $RRF_{2005,SR}$. Similar to the day-of-week changes, the largest differences were seen at the western monitors. Thus higher variability between both phenomena are predicted in the West. For example, HALC had a 6% and HROC had a 8% difference between $RRF_{2005,SR}$ and $RRF_{2005,FR}$. The difference in the fast and slow riser based O_3 predictions at the eastern monitors is nearly double the differences due to day-of-week changes. At the LYNF, SBFP, and WALV monitors the model was more responsive to changes in meteorology than to the emissions changes simulated here.

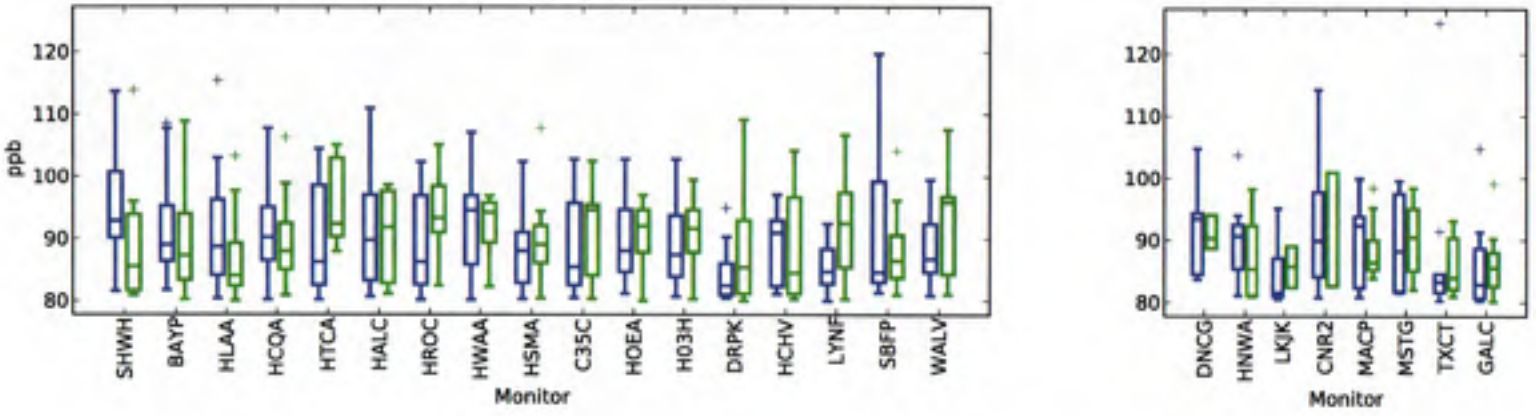

Figure 3.14: The box and whisker plot of the average of max 8-hr modeled concentrations for the base line case for slow riser (blue) and fast riser (green) by monitor. The plot extends from the lower to upper quartile values of the data, with a line at the median. Outlier points are those past the end of the whiskers and are only displayed if data point exsist outside upper and lower quartiles. Monitors are geographically divided into monitors that are (left) less than and (right) greater than 25 km from downtown Houston.

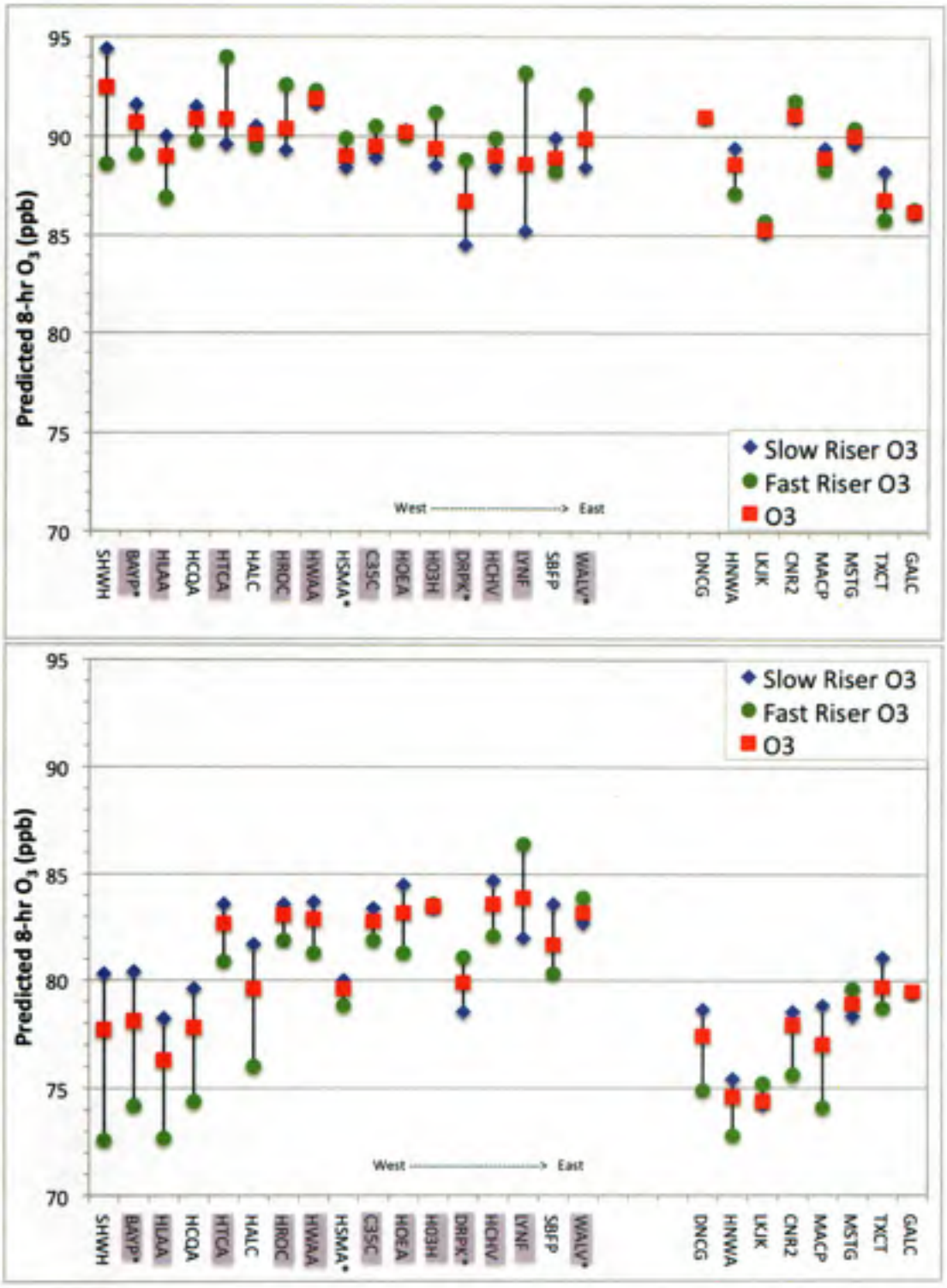

Figure 3.15: Base line episode (Top) and 2018 episode (Bottom) predicted daily max 8-hr modeled concentrations near a monitor averaged across all days (red), just slow risers (blue) and just fast risers (green) in ppb. Monitors are dived geographically between those monitors (left) less than and (right) more than 25 km from downtown Houston. Highlighted monitors are inside CHOU. Starred monitors failed TCEQ's attainment test .

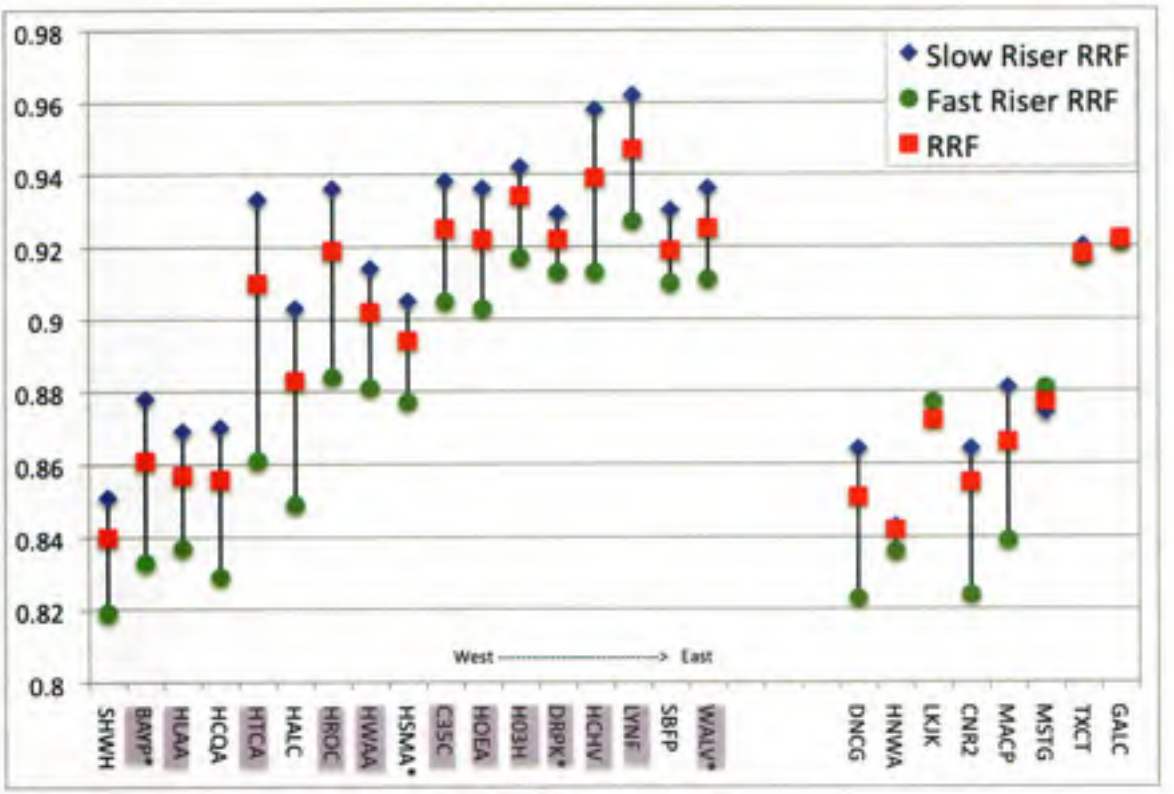

Figure 3.16: Relative reduction factor for all monitors calculated using all days (RRF_{2005}, red), and using just slow riser days ($RRF_{2005,SR}$, blue) or fast riser days ($RRF_{2005,FR}$, green). Monitors are ordered West to East and dived geographically between those monitors (left) less than and (right) more than 25 km from downtown Houston. Highlighted monitors are inside CHOU and starred monitors are in non-attainment.

Figure 3.17 shows for every monitor the DV_Fs calculated using RRF_{2005}, $RRF_{2005,SR}$, and $RRF_{2005,FR}$. A range of 3 ppb to 6 ppb between slow and fast riser DV_Fs is shown in the western side of CHOU from SHWH to HROC, where fast risers have the lower DV_F. A difference that ranged from 2 ppb to 4 ppb between slow risers and fast risers is observed in all other monitors. Two monitors that were in non-attainment, BAYP and HSMA, have slow riser DV_Fs that are in attainment. When compared to DV_F calculated using $RRF_{2005,WD}$ or $RRF_{2005,WE}$, the eastern monitors show larger reductions due to changes in the rise of the morning MMV height.

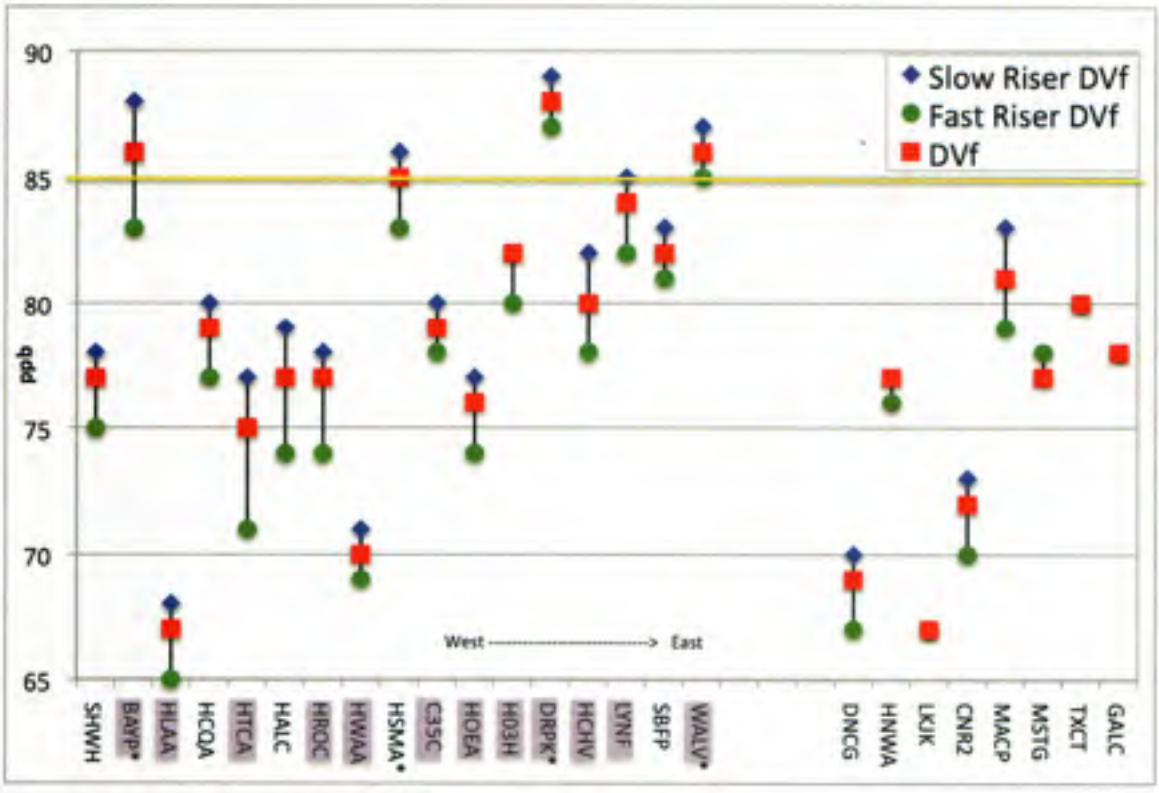

Figure 3.17: DV_F by monitor calculated using RRF_{2005} (red), $RRF_{2005,SR}$ (blue), and $RRF_{2005,FR}$ (green). Monitors are dived geographically between those monitors (left) less than and (right) more than 25 km from downtown Houston. Highlighted monitors are inside CHOU and starred monitors are in non-attainment.

3.3 Process Analysis Results

As shown previously, different MMV rise affects O_3 maximum values. Using process analysis techniques we will be able to quantify the changes in the chemical and physical processes that result from these different MMV profiles. We will also quantify whether O_3 production was produced under NO_x-limited or NO_x-inhibited conditions. Given the vast modeled data available for this analysis, we will limit the PA study to a slow rising weekday and weekend, and a fast rising weekday and weekend. This required finding representative days from the 413 modeled days. To complete this analysis we chose two representative meteorological phenomenon consisting of fast riser and slow risers, and applied them to the same EI from a weekday and a weekend

Table 3.3: Preliminary PA days including representative criteria

Date	Day of the Week	MMV Rise in CHOU	Max Ozone in CHOU (ppm)	Monitors in RRF_{2005}
05/21/05	Weekend	Slow	111	6
06/19/05	Weekend	Fast	105	7
06/21/05	Weekday	Slow	101	18
08/01/05	Weekday	Slow	144	24
08/06/05	Weekend	Fast	103	16
09/01/06	Weekday	Fast	127	18

resulting in four new-modeled days.

First criteria had to be developed so as to choose representative days. Days were chosen only if they were included by the TCEQ in their RRF_{2005} calculations and thus are policy relevant days. Thus, the search is narrowed to 120 simulation days of TCEQ's 2005 and 2006 episodes. Next, we chose days with the highest O_3 predictions. Principally, the top 3 highest O_3 days for the particular episode above 100 ppb were chosen. We also strived to include modeling days that were used to calculate an RRF_{2005} for multiple monitors. This allows us to investigate days that influence the calculation of the RRF_{2005} in many monitors. The results were six candidate episode days whose statistics are shown in the Table 3.3. This table portrays three candidates for each type of riser and day-of-the-week EI.

The next step of the analysis is to choose a weekday and a weekend from the pool of 6 model episode days to create 4 new simulations. Average profiles of NO_x and VOC for all these candidate PA days were also examined. Figure 3.18 shows the average emissions for these precursors for the CHOU from 7 to 18 LST in moles/hr. The VOC time series plot for Aug. 6 is in the median of the days in this group. The NO_x time series showed lower than average emissions, which is representative of a weekend. All these traits make it a good candidate as the sample weekend. A day

Table 3.4: In-house modeled PA day for analysis of type of riser for weekday and weekend EIs.

Day of the Week	MMV Rise in CHOU	Date of EI	Date of Met.
Weekday	Slow	06/21/05	08/01/05
Weekday	Fast	06/21/05	08/06/05
Weekend	Slow	08/06/05	08/01/05
Weekend	Fast	08/06/05	08/06/05

with a comparable VOC emission profile to Aug. 6, 2005 is June 21, 2005. Moreover, it has a high NO_x emission, making it a good candidate for weekday EI. In conclusion, the EIs used for this study are that of June 21 2005 and Aug. 6, 2005 for a weekday and weekend, respectively.

The details for choosing input meteorology mainly consisted in selecting two days with different early morning rises, but similar overall volumes. For example, September 1, 2006 had an average volume for the 8-18 LST of ~200 m/hr more than any candidate day at ~1400 m/hr. August 1 and August 6, 2005 had comparable hourly MMVs at ~1000 and ~1200 m/hr. The sunlight hours of these days, which plays a major factor in the rise and drop of MMV, are noticeably analogous. Figure 3.19 shows the MMV profile for these selected meteorological inputs.

Table 3.4 summarizes each new in-house modeled day. In brief, producing the modeled day consists of running CAMx with the selected EI and meteorology. It is important to point out that the initial conditions for each day correspond to the initial conditions of the EI input day and not the meteorology input. Using the initial conditions from the EI gives a better representation of the impact of the day-of-the-week, be it weekday or weekend, because the chemical composition of the day before is taken into account onto the current day. Finally, these compilations of days were run with PA to enable further investigation of chemistry and physical process.

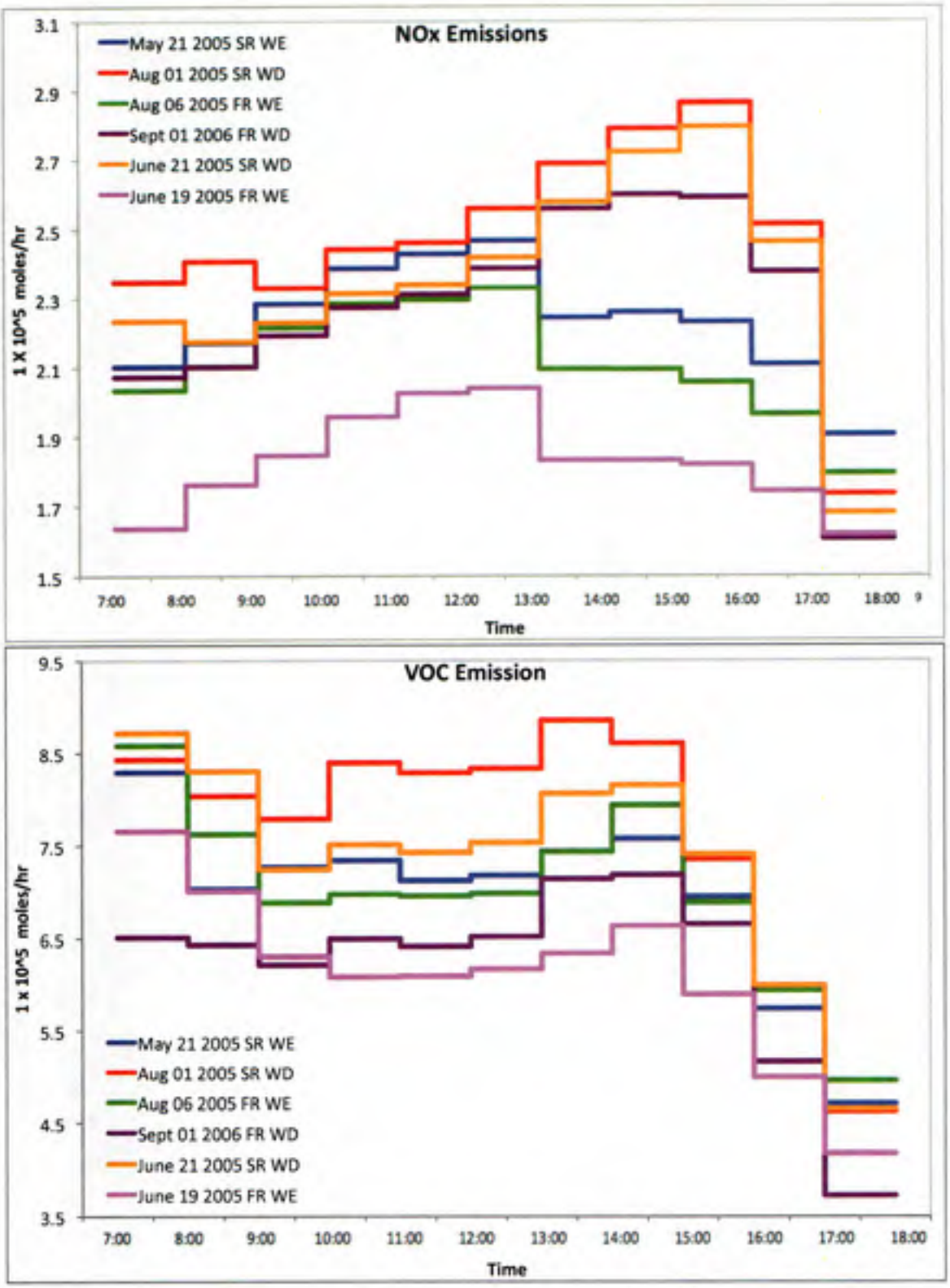

Figure 3.18: Emission rates for (Top) NO_x and (Bottom) VOC from CAMx EI inputs from 7 to 18 LST for preliminary PA days. The average hourly emissions were calculated for the CHOU domain from 7 to 18 LST in moles/hr.

Physical processes are effectively visualized through plots like those in Figures 3.19. This plots shows gains and losses from processes aggregated over the PA volume (CHOU subset horizontally and the MMV vertically) for every hour. It depicts physical processes such as entrainment, deposition, horizontal and vertical transport and dilution. It divides the chemistry process into aerosol chemistry and gas phase chemistry. It also displays emissions and the model concentration (Conc_Initial), which is the sum of all the gain and losses of the process.

Figure 3.19 portrays NO_x and VOC carbon (VOCC) for slow and fast riser on a weekday. It is important to recall that the emission inventory for both days is exactly the same, which is why both days begin with the same amount of each species. In the hours before 7 LST, the MMV is exactly the same between these two days. Between the hours of 5 and 8 LST, however, both NO_x and VOC concentration in the fast riser are higher than in the slow riser by 10 ppb and 50 ppb, respectively. This is due to vertical transport (V_trans) that carries species out of the PA volume. A more significant phenomenon occurs between hours 8 and 9 LST. A change in MMV of around 800 m/hr occurs in the fast riser. This causes a drop in the concentration of NO_x and VOCC due to dilution. This sharp MMV increase causes a NO_x decrease of more than 40 ppb between 8-10 LST. The same dilution phenomenon happens with VOCC. Even though there is addition of VOCC due to entrainment of material as the MMV rises, VOC concentrations decreases by more than 150 ppb.

In the slow riser there is a steady and smaller stepwise increase of the MMV. The MMV mean rise for the slow riser does not reach the height of the fast riser even at its peak of 1300 m at hour 14 LST. Consequently, concentrations are higher in the slow riser for both species. Only by hour 13 LST does the NO_x and VOC concentrations in the slow riser resemble that of the fast riser to within 2 ppb and 10 ppb, respectively.

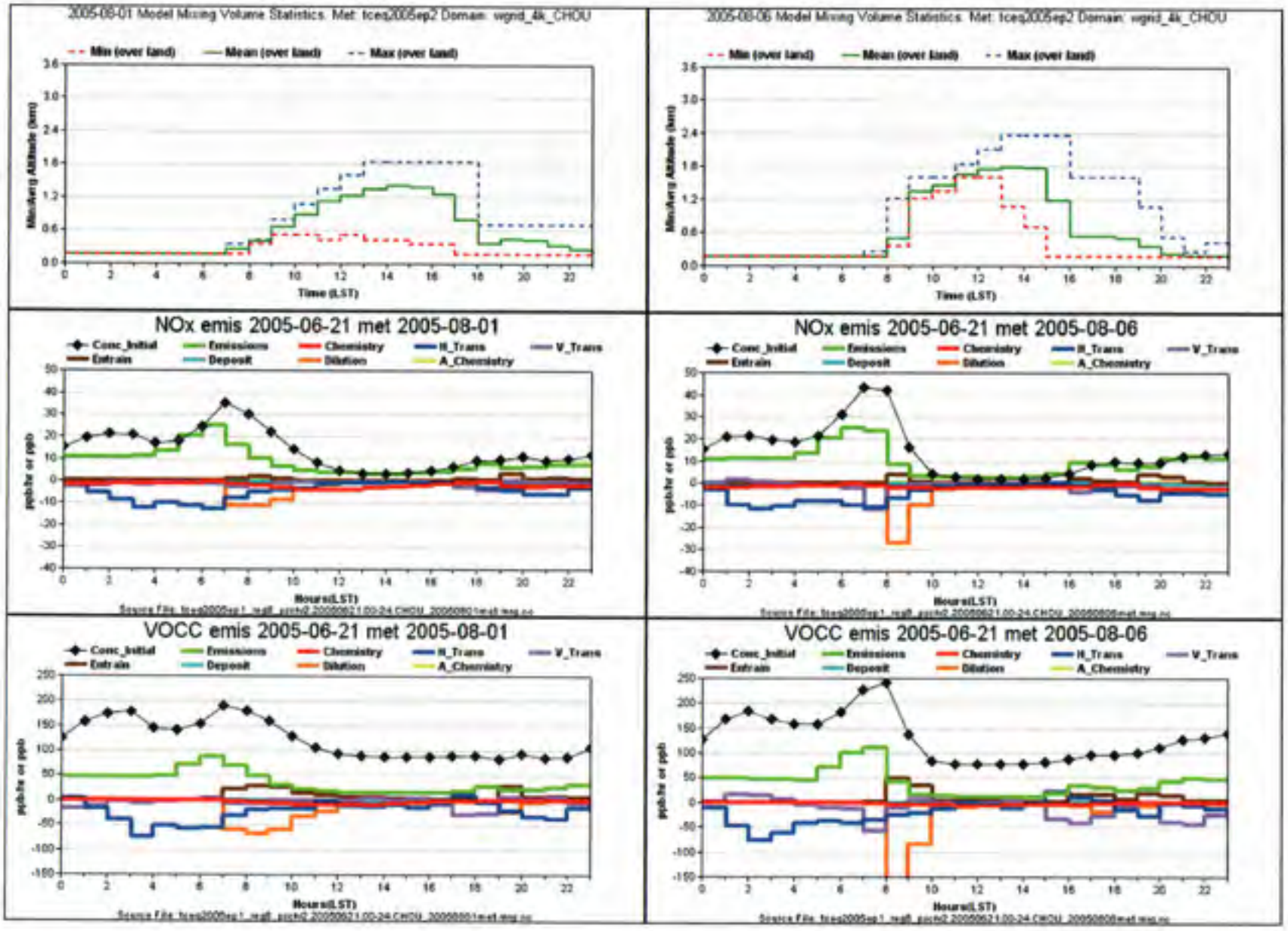

Figure 3.19: Evolution of MMV, NO_x and VOC carbon (VOCC) concentrations and rates of change over the course of a 24-hour in the CHOU domain for the weekday EI with (Left) slow riser and (RIght) fast riser.

After hour 14 LST, both MMVs begin to drop, and the fast riser mean drops much faster than the slow riser. By 16 LST ~66% of the mean MMV has dropped from the peak. The same drop does not occur until hour 18 in the slow riser. In both types of risers, NO_x begins to increase at hour 16 LST due to late afternoon mobile emissions. In the fast riser a steeper increase occurs, but after 6pm both NO_x concentrations are similar. A different trend is exhibited by VOC. In the late after noon, VOC remains relatively constant in the slow riser. In the fast riser it steadily increases as a consequence off entrainment of VOC species.

The rise of the MMV height has a significant affect on process rates. For example, at 8 LST there is s significant difference in MMV heights of nearly 900 m. This large difference results in a loss of nearly a 30 ppb of NO_x due to dilution processes and more than 150 ppb for VOCC. This causes a much steeper drop in O_3 concentrations in the fast riser day. The rapid rise on June 21 also caused an increase in the entrainment process bringing in both NO_x and VOCC from upper layers. These entrainment rates are nearly double those on the slow riser day. It is also clear from the NO_x concentrations that the CHOU domain runs out of NO_x at hour 10 LST in the fast riser, three hours earlier than in the slow riser. These data show that the MMV rise alter dilution and entrainment rates and has a significant change on O_3 precursor concentrations.

Changes in VOC and NO_x concentrations due to MMV rise have a considerable effect on O_3. Figure 3.20 shows the CHOU domain O_3 concentrations and process rates for a weekday fast and slow riser day. Before and after the photochemical day, O_3 is affected mainly by vertical and horizontal transport and chemical consumption in both the slow and the fast riser meteorology. The O_3 predicted on each of these days diverges when the photochemical day begins after 8 LST. At this time, the slow riser's O_3 concentration steadily increases due to entrainment and chemistry until almost 13

Table 3.5: Sum of all Physical Process from 8-18 LST for O_3 for Emission Inventory 6/21/05 using slow rising meteorology (8/1/05) and fast rising meteorology (8/6/05).

Meteorology Date	8/1/05	8/6/05
Emissions	0.0	0.0
Chemistry	96.4	74.3
Chemistry, gain	102.4	84.0
Chemistry, loss	-6.0	-9.7
Horizontal Transport	-47.2	32.6
Horizontal Transport, gain	23.7	82.8
Horizontal Transport, loss	-70.9	-50.3
Vertical Transport	-2.3	-63.6
Vertical Transport, gain	38.2	18.6
Vertical Transport, loss	-40.5	-82.3
Entrainment	121.4	120.2
Dilution	-105	-103
Deposition	-9.9	-9.1

LST and has a peak of 100 ppb. The fast riser, in contrast, has a concentration increase of 40 ppb from hours 8 to 10 (10 more ppb than the slow riser), mainly as a result of entrainment and transport. Figure 3.20, shows that the peak of chemical production during the photochemical day for the fast riser is not only earlier, but also about 50% lower then what was predicted using the slow riser meteorology. The chemical production of O_3 peaks at 11 LST in the fast riser day, two hours earlier than in the slow riser day. The reduction in morning NO_x concentrations appears to have caused O_3 production in the model to be lower, and forces it to peak earlier in the photochemical day.

Table 3.5 sums all the process rates from 8-18 LST for the weekday EI and a fast and slow riser meteorology. The data from the table show that the slow riser meteorology produced the most O_3 chemically. This day also saw larger losses due to horizontal transport, but less losses due to vertical transport. This is the result of of the MMV height collapsing sooner, and to a lower value on the fast riser day.

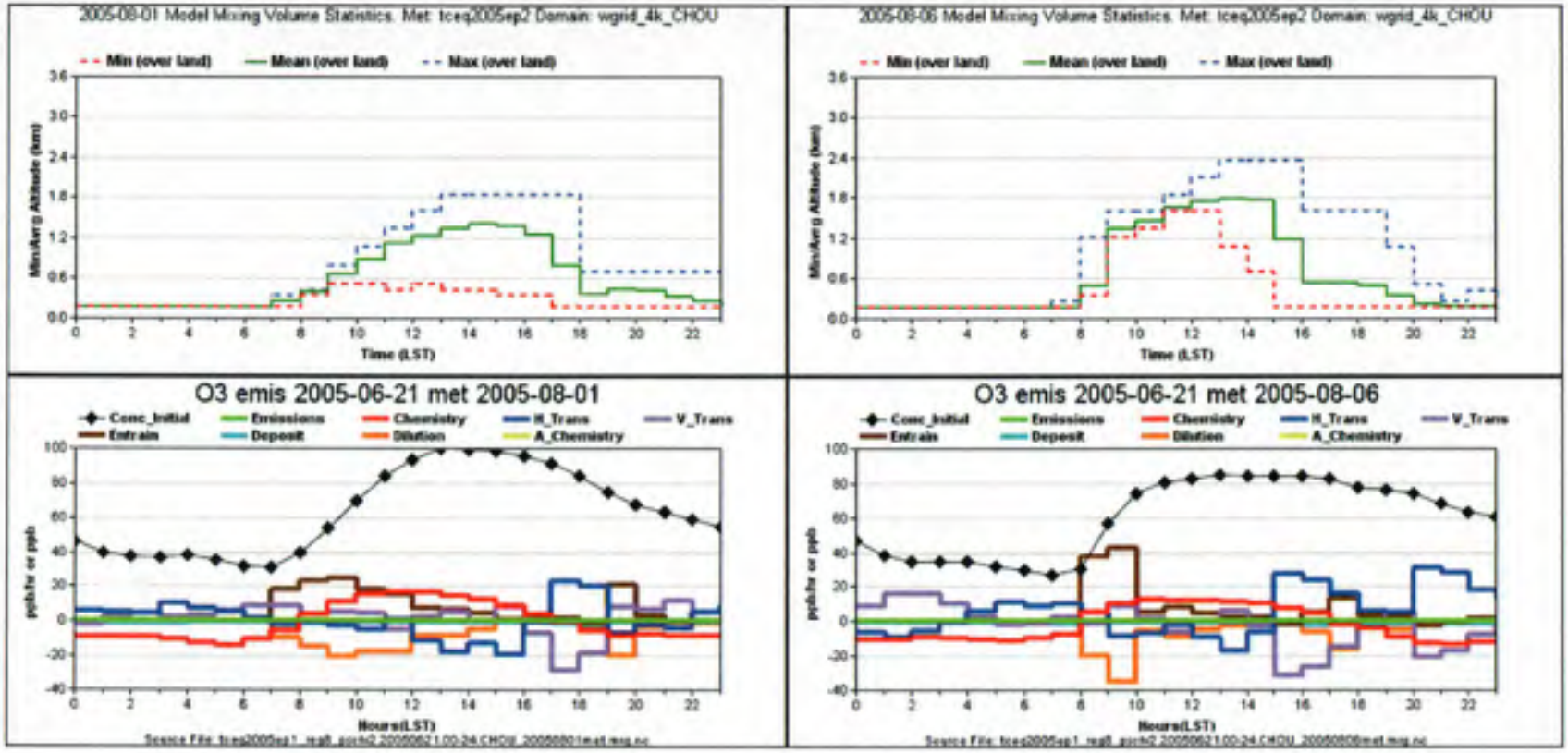

Figure 3.20: Evolution of MMV and O_3 concentrations and rates of change over the course of a 24-hour in the CHOU domain for the weekday EI with (Left) slow riser and (Right) fast riser.

There is substantial difference in the chemical process producing O_3 in the photochemical day between the slow and fast riser. The rapid rise in MMV height in the morning dilutes NO_x and VOC concentrations causing the day to run out of NO_x sooner. We now quantify the effect on chemical processes that this dilution has on O_3 production. Figure 3.21 summarizes key chemical parameters in the PA volume summed through out the photochemical day. These parameters have been described in detail in Jeffries and Tonnesen, 1994. This figure portrays several of the radical processes that are important to O_3 production. The chemical process chain that leads to O_3 production begins with radical initiation, or the production of new OH radicals. There are two sources of new OH radicals. Organic sources of new OH radicals include the photolysis of aldehydes and nitrous acid (HONO), and inorganic sources that involve production of OH through O_3 photolysis. In this analysis, for both meteorologies, the proportion of inorganic to organic new OH sources favors the inorganic sources. More than 65% of the new OH is due to inorganic sources. In the slow riser, however inorganic sources account for 3% more of the total new OH in comparison to the fast riser. This 3% difference accounts for more total new OH in the slow riser than the fast riser 47.2 and 41.7, respectively. Since the slow riser produced more O_3, more new OH radicals were made in this day.

The new OH radicals multiplied by the OH chain length (or the recycling of OH that occurs in VOC oxidation) is the total amount of OH that reacts with CO, VOC, and NO_2. In the slow riser, the OH chain length is 5% higher than the fast riser. Thus, the total OH reacted is 20% higher in the slow riser than the fast riser 124.5 and 105.1, respectively. The distribution of species that react with the OH radical is important to determine if the system terminates to end the cycle, or propagates to produces more O_3. If the cycle propagates, OH reactions oxidize CO and VOCs producing HO_2 and RO_2 radicals. In the slow riser, there is a 101 ppb reacting

with CO and VOCs compared to 88 ppb in the fast riser. Due to entrainment and transport the fast riser lost 60 ppb more VOC than the slow riser. From figure 3.21, the " OH + VOC by species" table shows the composition of VOC in both days. There is an overall decrease in the fast riser meteorology in the magnitude of VOC available to react with OH. Species that decrease by more than 20% are PAR, FORM, ETH, and OLE. The MMV heights also changed the amount of OH that terminated. The slow riser meteorology causes 14.9 ppb of OH to react with NO_2 and only 9.4 ppb in the fast riser case. At low NO_x concentrations a second, radical-radical, termination pathway that produces H_2O_2 becomes more important. Figure 3.21 shows that 12% more H_2O_2 was created in the fast riser than in the slow riser day. This is further evidence of the fast riser case becoming NO_x-limited. As a result of these reactions fast riser simulation produced 15% less NO_2 than the slow riser. This carries on to the photolysis of the NO_2, which leads to O_3 production. The slow riser produces 122 ppb of O_3, while the fast riser only produces 101 ppb of O_3. Similar results were seen with the weekend emissions as shown in Figure C.5 in appendix.

Additional analysis included the determination whether O_3 was produced under NO_x-limited or NO_x-inhibited conditions using two main radical termination pathways. The reaction of OH with NO_2 is a termination reaction that produces nitric acid (HNO_3) and usually occurs when NO_x is abundant. Under these conditions, O_3 production is limited by the rate at which radicals can be formed, which can be portrayed as the NO_x-inhibited regime. The reaction of HO_2 and RO_2 to form peroxides (H_2O_2) and other organic products is another main reaction that prevents propagation by NO to form O_3. This indicates that radical-radical reactions control the production of O_3. Under these conditions, O_3 production is limited by the availability of NO to react with HO_2 and RO_2 radicals, which is described as the NO_x-limited regime. Combining these two termination pathways enables to discern if the production of O_3 is NO_x-inhibited vs.

NO_x-limited, as proposed by Sillman (Sillman, 1995). Based on the ratio of peroxide production to nitric acid production, Sillman proposed that the transition between these conditions occurs at point related to the following ratio:

$$S.R. = \frac{P(H_2O_2)}{P(HNO_3)} \tag{3.1}$$

Where S.R. is the Sillman ratio, P(H_2O_2) is the production of hydrogen peroxide and P(HNO_3) is the production of nitric acid. When this ratio greater than 0.6 O_3 formation is NO_x-limited, when this ratio is less than 0.3 O_3 formation is NO_x-inhibited and a value between 0.3 and 0.6 indicates an intermediate (or a transition) regime (Sillman, 1995).

Figure C.3 shows production rates of $HNO_3$and H_2O_2 and the corresponding Sillman ratio for the photochemical day with the slow riser and the fast riser meteorology in a weekday EI. The slow riser and the fast riser are fairly similar until 10 LST where the fast riser Sillman ratio starts increasing faster than the slow riser. At this time the fast riser has a smaller concentration of NO_x and thus begins to become NO_x-limited. This phenomenon coincides with a drop in HNO_3production in the fast riser simulation. The slow riser simulation does not enter the transition region until after 13 LST and is only in the NO_x-limited region during 14-15 LST. The two indicators converge at 16 LST. This is the time when the MMV begins to drop in the fast riser, as seen in Figure 3.19. Thus, NO_x concentrations are increased due to the considerably smaller volume. The Sillman ratio decreases fast enough that at 17 LST the fast riser is more NO_x-inhibited than the slow riser. By the end of the day, both risers have similar NO_x-inhibition. The weekend day showed similar patterns, but due to lower emissions overall magnitudes were lower (Figure C.2).

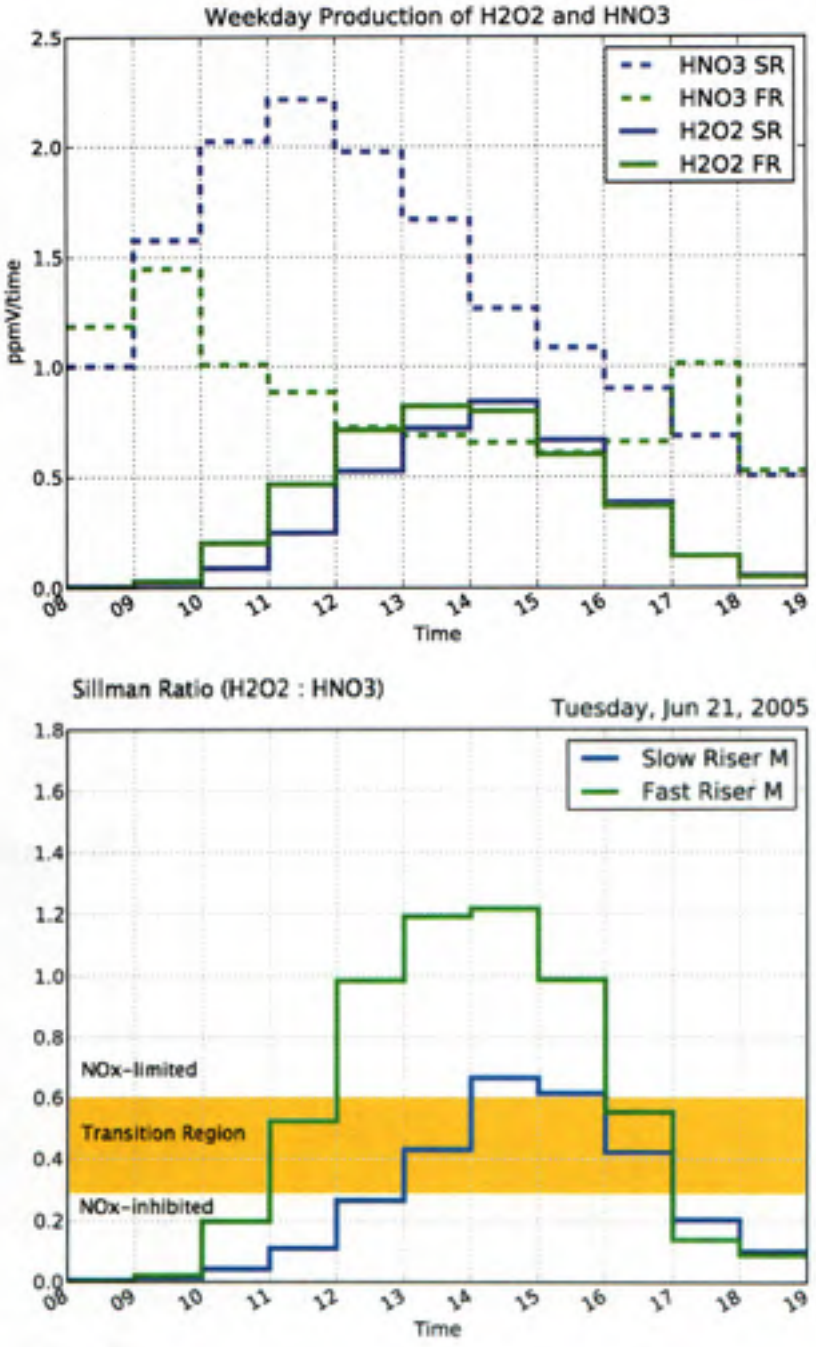

Figure 3.22: (Top) Hourly production of $HNO_3$and H_2O_2 and (Bottom) Sillman Ratio from 8 to 18 LST for Slow Riser (SR) and Fast Riser (FR) for the weekday EI

In summary, the fast riser phenomenon can cause a day to become NO_x-limited much earlier in the day than the slow riser, thus restraining O_3 production by NO_x availability. The same effect is depicted for weekends, where less production of O_3 in the fast riser weekend and a NO_x-limited regime much earlier than the slow riser is observed to a very similar degree (For NO_x, VOCC and O_3 profiles as well as Sillman ratios for weekends review appendix figures C.2 and C.4). This meteorology phenomenon, in conclusion, may result in the same EI giving distinctly different O_3 producing regimes and thus affect the type of controls needed to reduce O_3 in CHOU.

CHAPTER 4

SUMMARY AND CONCLUSIONS

This work has developed an investigation of the modeling based attainment metric, relative reduction factor (RRF_M) for O_3. The main goal of the study was to understand the implications of the averaging technique for calculating the RRF_M using as a dataset the TCEQ 2005, 2006, and 2018 regulatory simulations. The dataset is comprised of 63 simulated days that contain days with maximum daily 8-hour O_3 concentrations above 85 ppb used by TCEQ for calculating the RRF_{2005} to test future attainment of 25 monitors. The study of these days primarily focused on the most photochemically active area, which encompasses both the Houston Ship Channel and downtown Houston as shown in Figure 2.4. For this central Houston domain, labeled CHOU, the 63 modeling days were used to quantify the sensitivity of O_3 production to changes in precursor concentrations due to human activity and in morning MMV rise.

Overall findings show that the model's response to changes in precursor concentrations depend on geographical location. This means that the CHOU contains distinct areas of O_3 production with NO_x-inhibited and NO_x-limited regimes. In areas of concentrated mobile emissions, for example, weekend human activity results in an average NO_x reduction of 13%. Throughout most of the domain, this reduction results in lower O_3 concentrations by as much as 8 ppb. In eastern Houston, however, where monitors are affected by industrial emissions and where there is a constant supply of NO_x throughout the week, higher O_3 was predicted. Such results indicate a NO_x-inhibited weekend environment. In the 2018 simulation, the western side of Houston had the

largest reductions in O_3 with RRF_{2005} as low as 0.82. The eastern side of Houston appears to be "stiffer" to reductions with RRF_{2005} closer to 0.92. For any given monitor, up to 40% of days used for the RRF_{2005} had a variability in O_3 predictions of up to 35 ppb. At every monitor, weekend days were more responsive to controls than weekdays resulting in a variability in RRF_{2005} of up to 0.07. This implies that in weekends where less NO_x is produced than weekdays the response to controls are greater.

In addition, precursor concentrations also vary with MMV morning rise. Two unique meteorological patterns that affect the MMV and O_3 production were observed. The TCEQ's 63 modeling days were classified according to MMV rise using the CHOU wide domain. MMVs were considered a rapid riser if the MMV height change was greater than 700 m/hr between the hours of 6-11 LST, and a slow riser if less than that rate. Process analysis results showed that the rapid rise of the MMV results in more than five times higher dilution rates of O_3 precursors causing a steeper O_3 production rate in the morning. This resulted in a earlier and lower concentration peak of O_3 in the fast riser compared to the slow riser. The study of fast risers portrays an abrupt change to the NO_x-limited regime, where radicals begin to self terminate in the late afternoon producing H_2O_2. Thus, the response to these reductions in precursor concentrations was similar to the day of week analysis where the western side of Houston saw the largest reductions in O_3 and the eastern side had RRF_{2005} near 0.92. For any given monitor, up to 51% of days used for the RRF_{2005} were fast riser days. This means inclusion of modeling days where O_3 concentrations can vary by as much as 35 ppb and deviate an RRF_{2005} by as much as 0.07.

These results suggest that Houston is a complex environment in which distinct areas respond differently to across the board controls. Thus, this implies that there are several ways to produce high O_3 in Houston, each requiring a unique control

strategy. The averaging together of these phenomena results in an artificial response where, in many cases, it is less responsive than actual conditions.

BIBLIOGRAPHY

ALA. State of the air report: 2004, 2004. URL http://lungaction.org/reports/sota04_full.html.

American Lung Association ALA. Air pollution facts and air quality info - best and worst cities - ala state of the air 2007, 2007. URL http://lungaction.org/reports/sota07_cities.html.

David Allen, Cynthia Murphy, Yosuke Kimura, William Vizuete, Thomas Edgar, Harvey Jeffries, Byeong-Uk Kim, Mort Webster, and Michael Symons. Variable industrial VOC emissions and their impact on ozone formation in the Houston Galveston area. Technical report, Texas Environmental Research Consortium, April 2004. URL http://files.harc.edu/Projects/AirQuality/Projects/H013.2003/H13FinalReport.pdf.

C. Blanchard, S. Tanenbaum, and D. Lawson. Differences between weekday and weekend air pollutant levels in Atlanta; Baltimore; Chicago; Dallas-Fort Worth; Denver; Houston; New York; Phoenix; Washington, DC; and surrounding areas. *Journal of Air and Waste Management Association*, 58:1598–1615, 2008.

Daewon W. Byun. UH IMAQS air quality forecasting model configurations, May 2007. URL http://imaqs.uh.edu/ModelSetup.html.

D.W. Byun and J.K.S. Ching. Science algorithms of the EPA Models-3 Community Multiscale Air Quality (CMAQ) modeling system. Technical report, Office of Research and Development, US Environmental Protection Agency, Washington, DC, 1999. EPA Report N. EPA-600/R-99/030.

D.W. Byun, Soontae Kim, Hyun-Cheol Kim, Fong Ngan, Beata Czader, Xiangshang Li, In-Bo Oh, Dae-Gyun Lee, Fang-Yi Cheng, , and Peter Percell. Retrospective Simulations of TexAQS II-2006 Pollution Events HARC Project H87 Final Report. Technical report, University Houston, December 2007. URL http://files.harc.edu/Projects/AirQuality/Projects/H087/H087FinalReport.pdf.

ENVIRON. *User's Guide CAMx Comprehensive Air Quality Model with Extensions Version 4.20*, 2005. URL www.camx.com.

EPA. Guidance on the use of models and other analyses for demonstrating attainment of air quality goals for ozone, pm2.5, and regional haze. Technical Report EPA - 454/B-07-002, Environmental Protection Agency, 2007.

EPA. Federal Register 40 CFR Parts 50 and 58 National Ambient Air Quality Standards for Ozone; Final Rule. Technical report, Environmental Protection Agency, 2008a.

EPA. Health and environment, 2008b. URL http://www.epa.gov/air/ozonepollution/health.html.

U.S. EPA. Community Multiscale Air Quality (CMAQ) science documentation. Technical report, U.S. Environmental Protection Agency, 2006. URL `http://www.epa.gov/asmdnerl/CMAQ/index.html`.

G. Grell, J. Dudhia, and D. Stauffer. A description of the fifth-generation Penn State/NCAR mesoscale model (MM5). Technical report, National Center For Atmospheric Research, 1995. Technical Note (NCAR/TN-398 + STR).

B Henderson. The influence of model resolution on ozone from industrial VOC releases. M.S. Thesis, University of North Carolina, Chapel Hill, NC, Jan 2008. URL `http://gradworks.umi.com/14/52/1452937.html`.

J. M. Heuss, D. F. Kahlbaum, and G. T. Wolff. Weekday/weekend ozone differences: What can we learn from them? *Journal of Air and Waste Management Association*, 53:772–788, 2003.

C. Hogrefe, K. L. Civerolo, W. Hao, J. Y. Ku, E. E. Zalewsky, and G. Sistla. Rethinking the assessment of photochemical modeling systems in air quality planning applications. *Journal of the Air and Waste Management Association*, 58(58):1086–1099, 2008.

R. B. Husar. Seasonal and weekly pattern of ozone over the otag region. paper presented at Air and Waste Management Association's 90th Annual Meeting & Exhibition, 1998.

H. E. Jeffries and S. Tonnesen. A comparison of two photochemical reaction mechanisms using mass balance and process analysis. *Atmospheric Environment*, 28(18): 2991–3003, 1994.

J. M. Jones, C. Hogrefe, R. F. Henry, J. Y. Ku, and G. Sistla. An assessment of the sensitivity and reliability of the relative reduction factor approach in the development of 8-hr ozone attainment plans. *Journal of the Air and Waste Management Association*, 55(1):13–19, 2005.

D. Karp. Initial 2018 HGB modeling results. Presentation made September 26, 2008, 2008.

Yosuke Kimura, Elena McDonald-Buller, William Vizuete, and David T. Allen. Application of a lagrangian process analysis tool to characterize ozone formation in southeast Texas. *Atmospheric Environment*, 2007.

John W. Nielsen-Gammon. Meteorological modeling for the august 2000 houston-galveston ozone episode: Pbl characteristics, nudging procedure, and performance evaluation. Technical report, Department of Atmospheric Sciences, Texas A&M University, February 2002.

V. Pont and J. Fontan. Interactive discussion comparison between weekend and weekday ozone concentration in large cities in France. *Atmospheric Environment*, 35:1527–1535, 2001.

S. C. Pryor and D. G. Steyn. Hebdomadal and diurnal cycles in ozone time-series from the lower Fraser Valley, BC. *Atmospheric Environment*, 29:1007–1019, 1995.

B. K. Pun, C. Seigneur, and W. White. Day-of-week behavior of atmospheric ozone in three us cities. *Journal of Air and Waste Management Association*, 53:789–801, 2003.

S Sillman. The use of NO_y, H_2O_2, and HNO_3 as indicators for ozone-NO_x-hydrocarbon sensitivity in urban locations. *J. Geophys. Res.*, 100(D 7):14175–14188, 1995.

G. Sistla, C. Hogrefe, W. Hao, J. Y. Ku, E. Zalewsky, R. F. Henry, and K. Civerolo. An operational assessment of the application of the relative reduction factors in the demonstration of attainment of the 8-hr ozone national ambient air quality standard. *Journal of the Air and Waste Management Association*, 54(8):950–959, 2004.

J. Smith, M. Estes, F. Mercado, and J. Mellberg. Assessing model performance using weekday/weekend analysis. Presented at the 6th Annual CMAS Conference, 2007.

TCEQ. SIP Revision: Houston-Galveston-Brazoria; Ch. 101 and Ch. 115 Rules, 2004. URL `http://www.tceq.state.tx.us/implementation/air/sip/dec2004hgb_mcr.html`.

TCEQ. Houston-galveston-brazoria eight-hour ozone sip modeling (2005, 2006 episodes): Camx modeling domain, 2005. URL `http://www.tceq.state.tx.us/implementation/air/airmod/data/hgb8h2/hgb8h2_camx_domain.html`.

TCEQ. Texas commission on environmental quality air monitoring sites, 2009a. URL `http://www.tceq.state.tx.us/nav/eq/mon_sites.html`.

TCEQ. Houston-galveston-brazoria ozone sip mid-course review modeling, 2009b. URL `http://www.tceq.state.tx.us/implementation/air/airmod/data/hgb1.html`.

TCEQ. Texas commission on environmental quality 2004 air pollution events, 2009c. URL `http://www.tceq.state.tx.us/assets/public/compliance/monops/air/sigevents/04/040918ani-houo3.html`.

TCEQ. Houston-Galveston-Brazoria eight-hour ozone sip modeling (2005, 2006 episodes), 2009d. URL `http://www.tceq.state.tx.us/implementation/air/airmod/data/hgb8h2/hgb8h2.html`.

R. Thomas. HGB modeling update 2005 baseline emissions. Presentation made February 18, 2008, 2008.

W. Vizuete, H. Jeffries, E. Christoph, B. Henderson, H. Parikh, and A. Valencia. Multi-resolution simulation and analysis of TexAQS II air pollution events. Technical report, University of North Carolina, December 2007. URL `files.harc.edu/Projects/AirQuality/Projects/H087/H087UNCFinalReport.pdf`.

F. Vukovich and J. Scarborough. 15-year simulation of ozone in Baltimore using SIPM. *Atmospheric Environment*, 38:4825–4837, 2004.

F. M. Vukovich. The spatial variation of the weekday/weekend differences in the Baltimore area. *Journal of Air and Waste Management Association*, 50:2067–2072, 2000.

G. Yarwood, J. Granta, B. Kooa, and A. Dunkerb. Modeling weekday to weekend changes in emissions and ozone in the Los Angeles basin for 1997 and 2010. *Atmospheric Environment*, 42:3765–3779, 2008.

APPENDIX A

MODEL SPECIFICATION

MET Inputs :

MM5 v3.7.3 for all domains - eta_dbemis_fddats_uhsst_utcsrlulc:

- Grell cumulus schemes for 108, 36, and 12km domains; no cumulus scheme for 4km domain
- RRTM radiation
- NOAH Land Surface Model (LSM) with TFS Texas Forest Service (TFS) land-duse data
- eta: ETA PBL Scheme for 4km domain
- dbemis: NASA derived emissivities for 4km domain
- fddats: analysis nudging for 108, 36, and 12km domains; observational nudging with profiler data for 4km domain with time-shift
- newSTIdata: updated observed data from STI - used in FDDA
- uhsst: UH hourly sea surface temperature
- utcsrlulc - UTCSR land use and land category data for 4km domain
- MM5 to CAMx conversion: mm5camx v4.5, TKE Kv scheme for all domains (min Kv= 0.1)

Domain Specifications:

The model domain is as described by the Texas Commission for Environmental Quality (TCEQ) for 2005, 2006 Houston-Galveston-Brazoria eight-hour ozone SIP modeling (HGB8H2). A map of the grids, as provided by TCEQ, is shown in Figure A.1. The horizontal grids are described in Table A.1 and their Lambert Conformal Conic projection is defined by the parameters listed in Table A.2. Table A.3 provides detailed vertical domain information, including figures of the course and fine CAMx vertical grid configurations, provided by TCEQ.

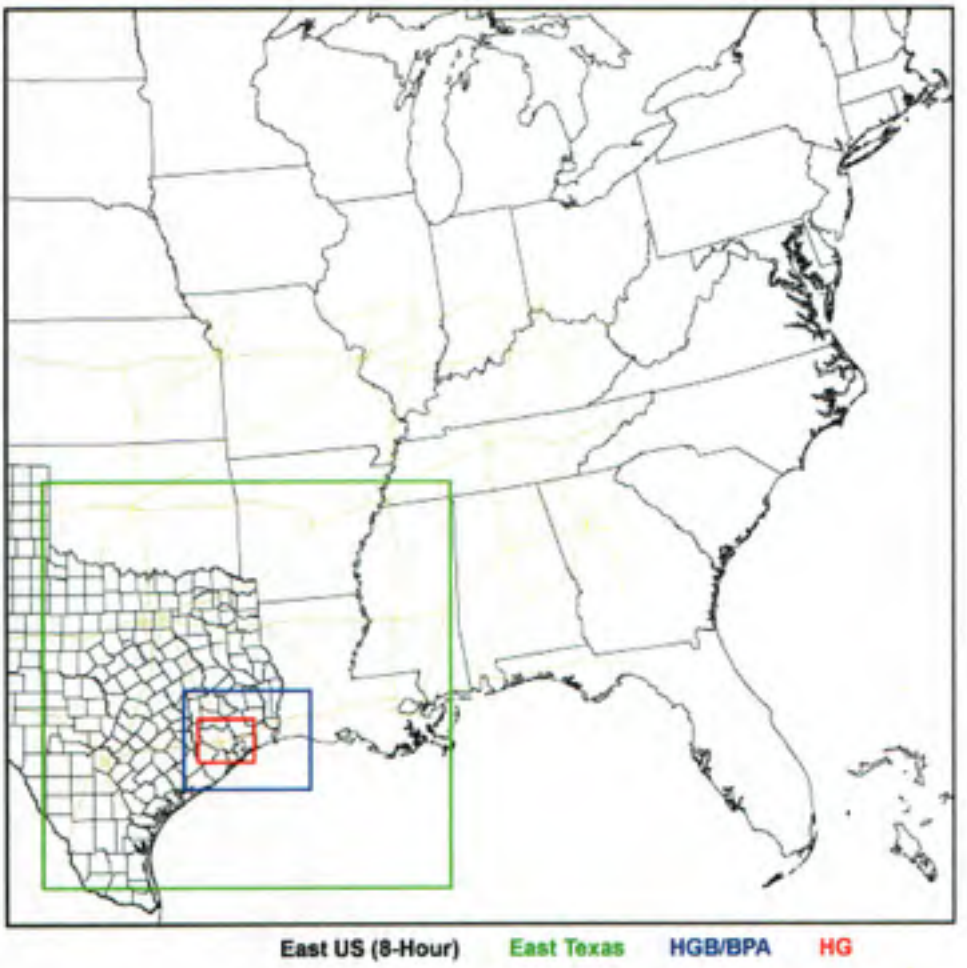

Figure A.1: CAMx modeling domains. Courtesy TCEQ.

Table A.1: Domain descriptions. Courtesy TCEQ.

Domain Name	Range (km)		Number of Cells		Cell Size (km)		Name in CAMx
	Easting	Northing	Easting	Northing	Easting	Northing	
East US Domain	(-108,2376)	(-1584,828)	69	67	36	36	eus_36km
East Texas Subdomain	(-12,1056)	(-1488,-420)	89	89	12	12	etx_12km
HGB/BPA Subdomain	(356,688)	(-1228,-968)	83	65	4	4	hgbpa_04km
HG Subdomain	(394,542)	(-1154,-1042)	74	56	2	2	hg_02km

Table A.2: Lambert Conformal Conic projection parameters.

Property	Value (°)
Central Meridian	-100
Central Longitude	-100
Center Latitude	40
Standard Parallel 1	30
Standard Parallel 2	60

Table A.3: Vertical modeling profiles. Figures courtesy TCEQ.

MM5 Layer	Layer Top (m AGL)	REG and ETX domains			HGA domain		
		CAMx Layer	Layer Thickness (m)		CAMx Layer	Layer Thickness (m)	
27	5835.9	15	1729.5	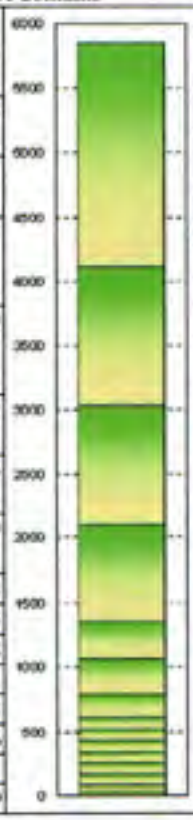	24	937.9	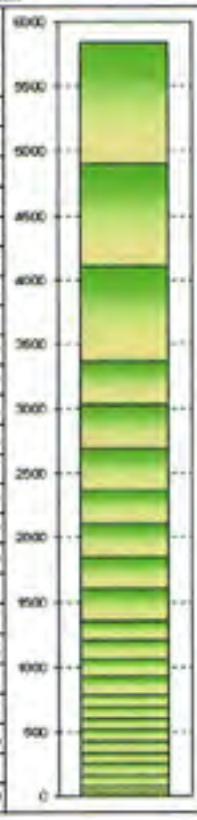
25	4898				23	791.6	
23	4106.4	14	1080.1		22	732.9	
21	3373.5				21	347.2	
20	3026.3	13	923		20	335.9	
19	2690.4				19	324.3	
18	2366.1				18	262.8	
17	2103.3	12	749.9		17	256.1	
16	1847.2				16	249.9	
15	1597.3				15	243.9	
14	1353.4	11	285.2		14	143.6	
13	1209.8				13	141.6	
12	1068.2	10	277.6		12	139.7	
11	928.5				11	137.9	
10	790.6	9	180.9		10	90.9	
9	699.7				9	90	
8	609.7	8	89.4		8	89.4	
7	520.3	7	88.5		7	88.5	
6	431.8	6	87.8		6	87.8	
5	344	5	87.1		5	87.1	
4	256.9	4	86.3		4	86.3	
3	170.6	3	85.6		3	85.6	
2	85	2	51.1		2	51.1	
1	33.9	1	33.9		1	33.9	

Note: AGL – above ground level.

APPENDIX B

WEEKDAY-WEEKEND ANALYSIS

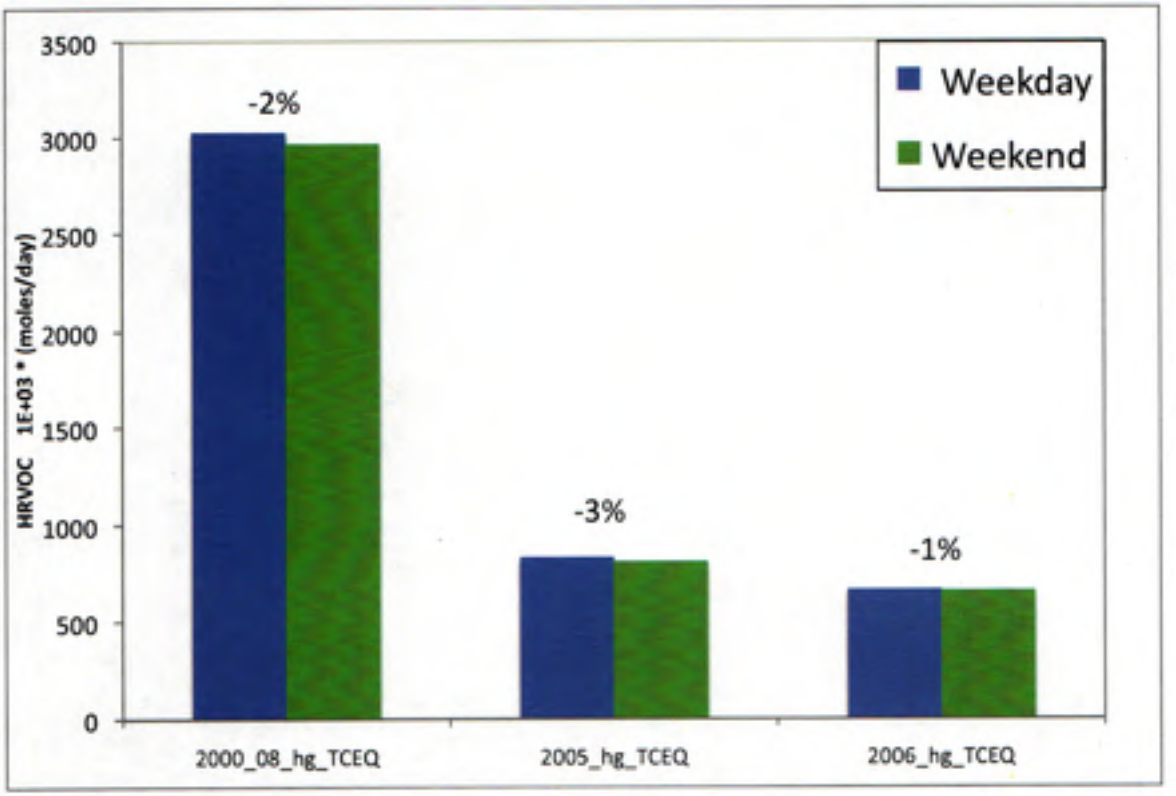

Figure B.1: Weekday and weekend HRVOC Emission rates for the 2000, 2005, and 2006 base case emission inventories. These emission rates are calculated by averaging the daily emission rates for all weekdays and again for only weekend days across all episode days.

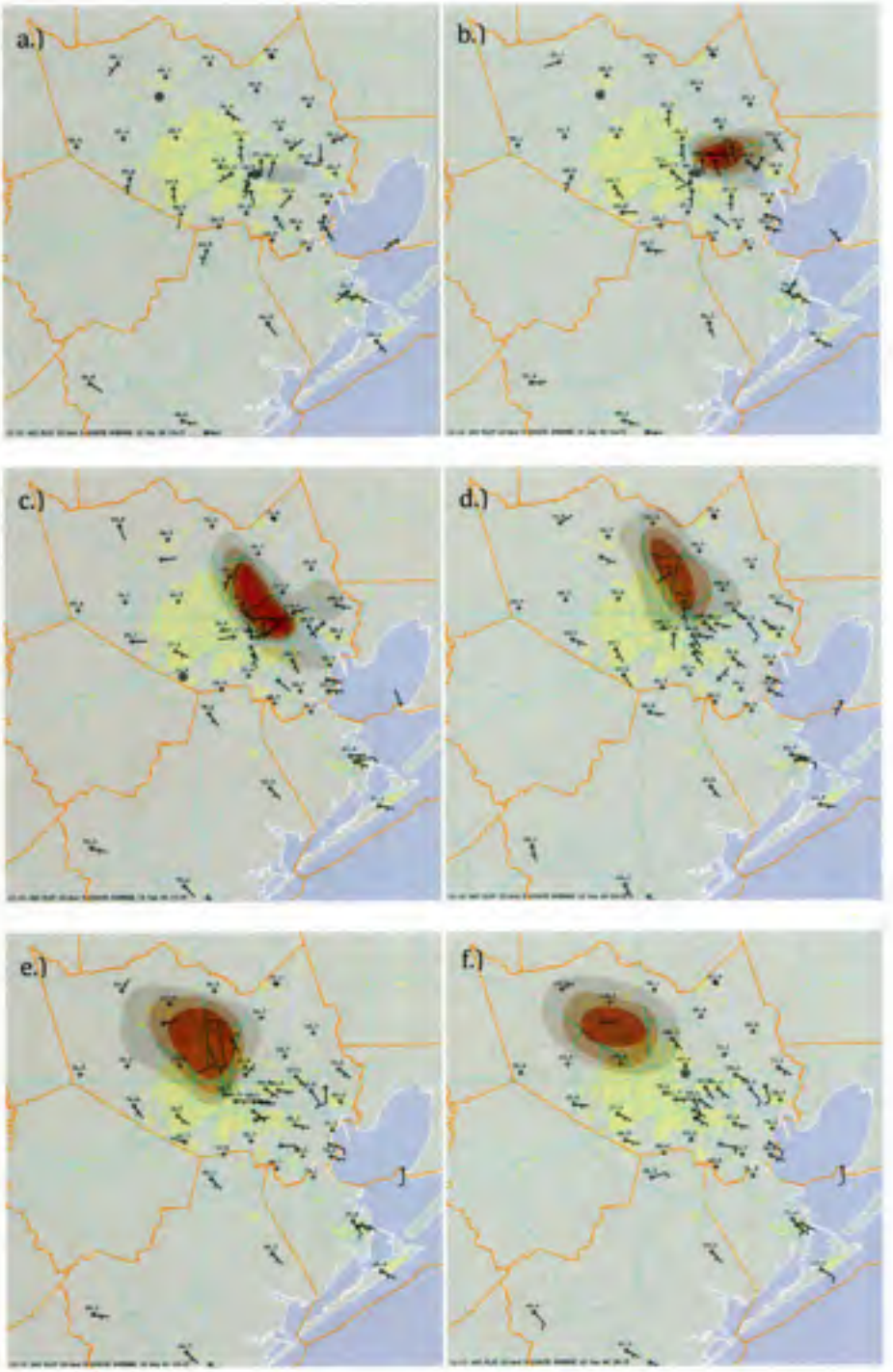

Figure B.2: Observed O_3 concentrations (ppb) from the TCEQ over Houston, Texas on September 18, 2004 from 1015 to 1515 CST. The figures are at 1-h intervals. Each figure shows the ozone concentration at that time, not the previous hours average. The high O_3 formed in a small region over the north side of the ship channel and was advected northward and then westward where it impacted the HNWA monitor. Ozone formation over the rest of the city was minimal. TCEQ, 2009c.

APPENDIX C

METEOROLOGICAL ANALYSIS

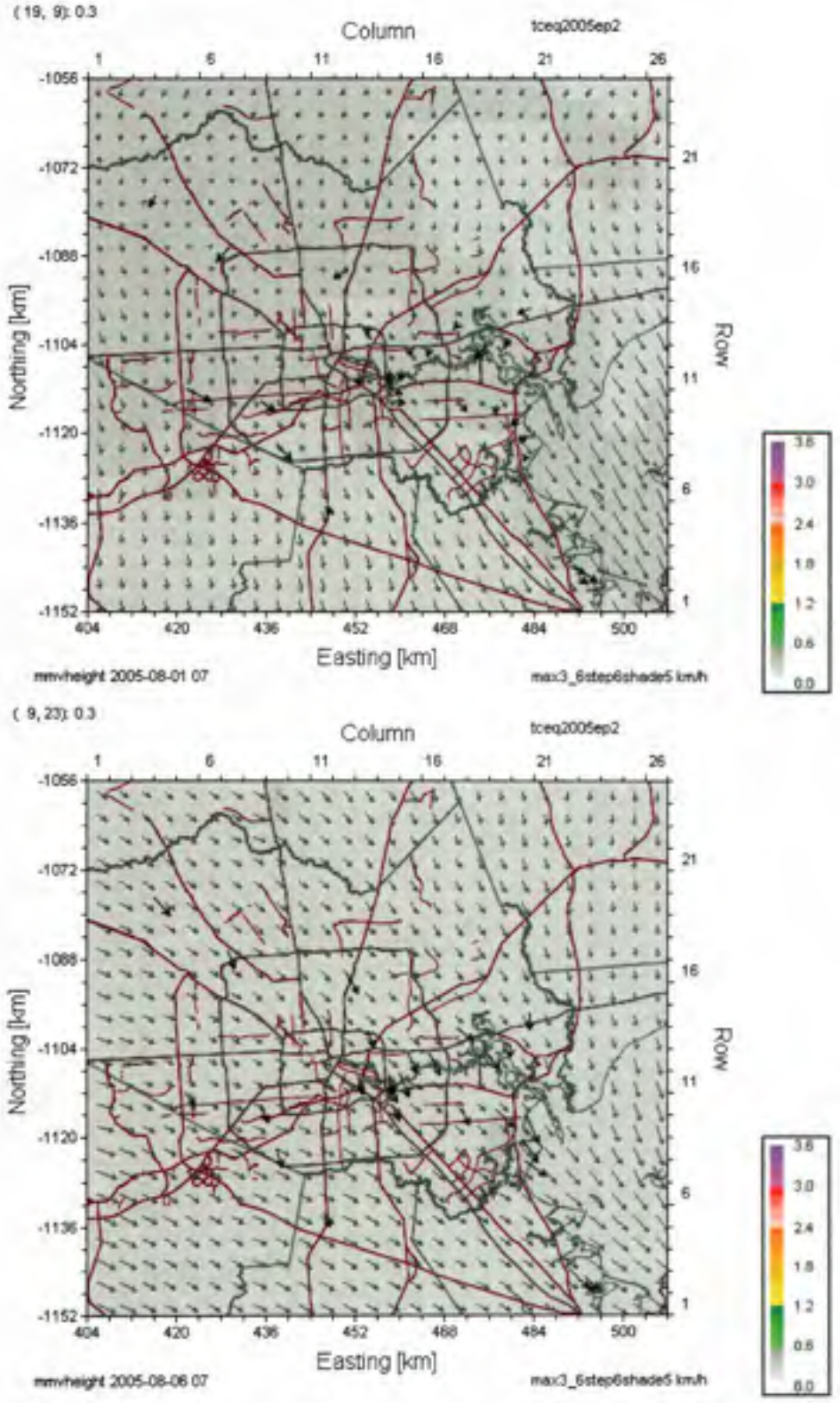

Figure C.1: MMV height (km) Spatial Tile plot for the 4km windowed domain for slow riser (left) 08/01/05 and fast riser (right) 08/06/05 at 7 am. The tan and grey lines represent highways systems and roads. The arrows represent hourly average wind direction.

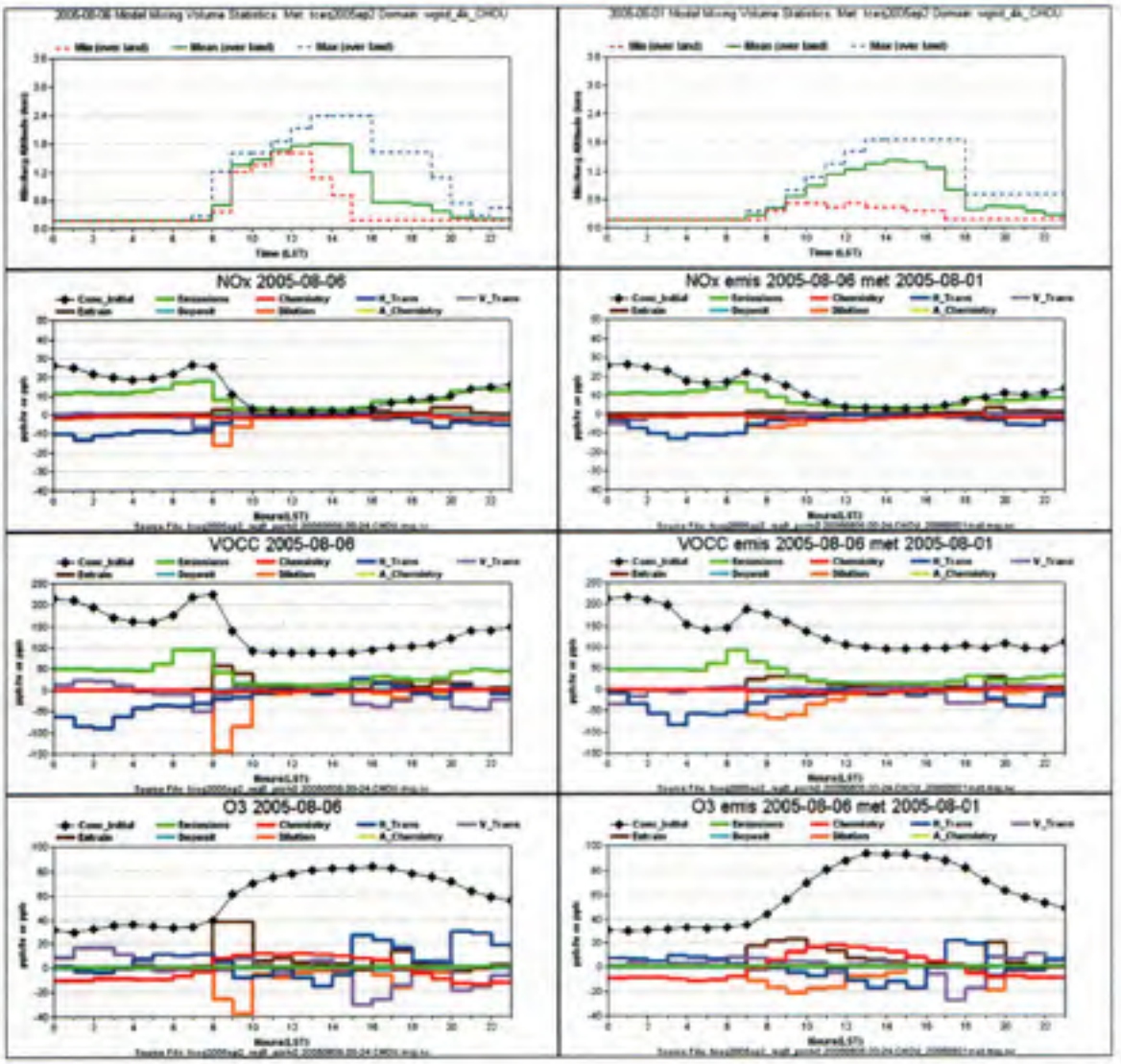

Figure C.2: Evolution of MMV, NOxVOC carbon (VOCC) and O_3 concentrations and rates of change over the course of a 24-hour in the CHOU domain for the weekend EI with (a) slow riser and (b) fast riser.

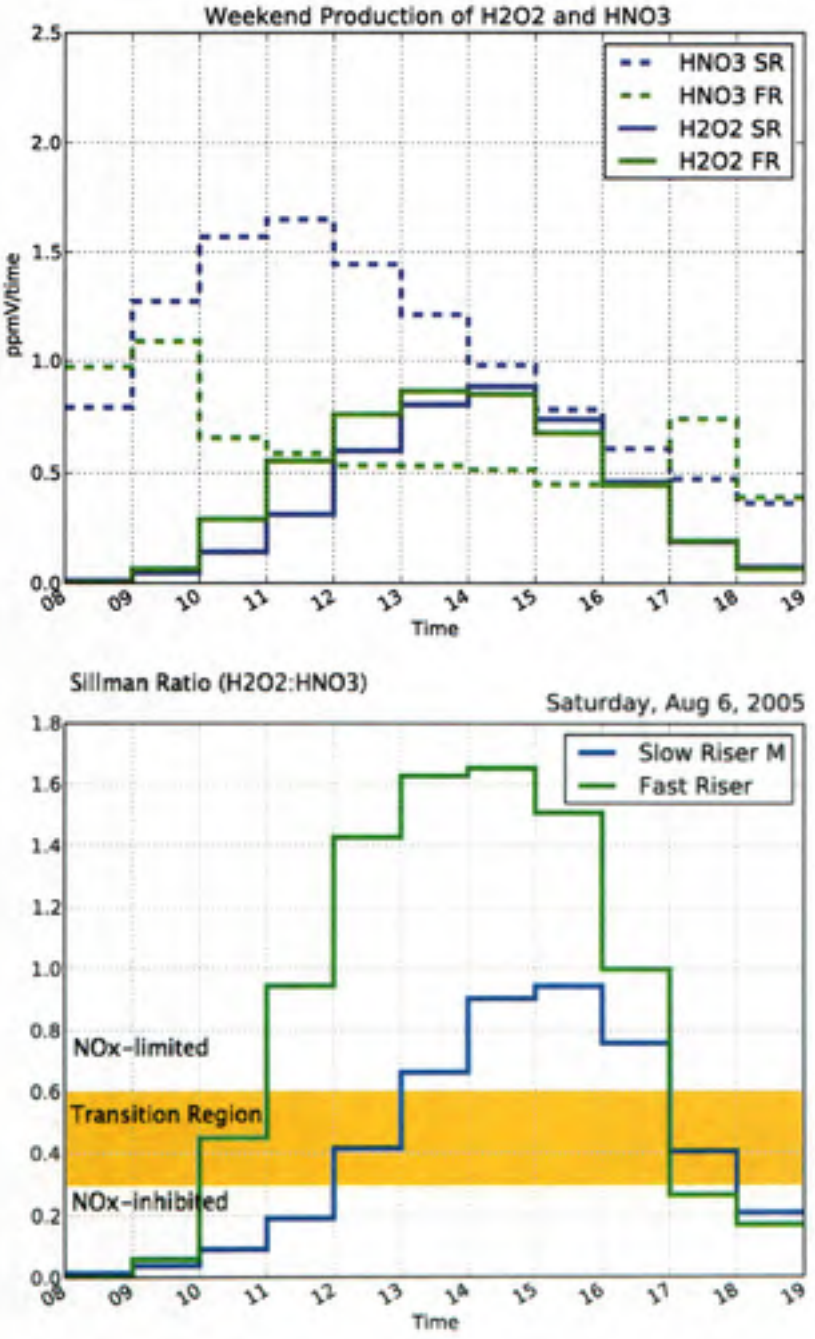

Figure C.3: (Top) Hourly production of HNO_3 and H_2O_2 and (Bottom) Sillman Ratio from 8 to 18 LST for Slow Riser (SR) and Fast Riser (FR) for the weekday EI

Figure C.4: Hourly Sillman Ratio from 8 to 18 LST for Slow Riser (SR) and Fast Riser (FR) for the weekend EI

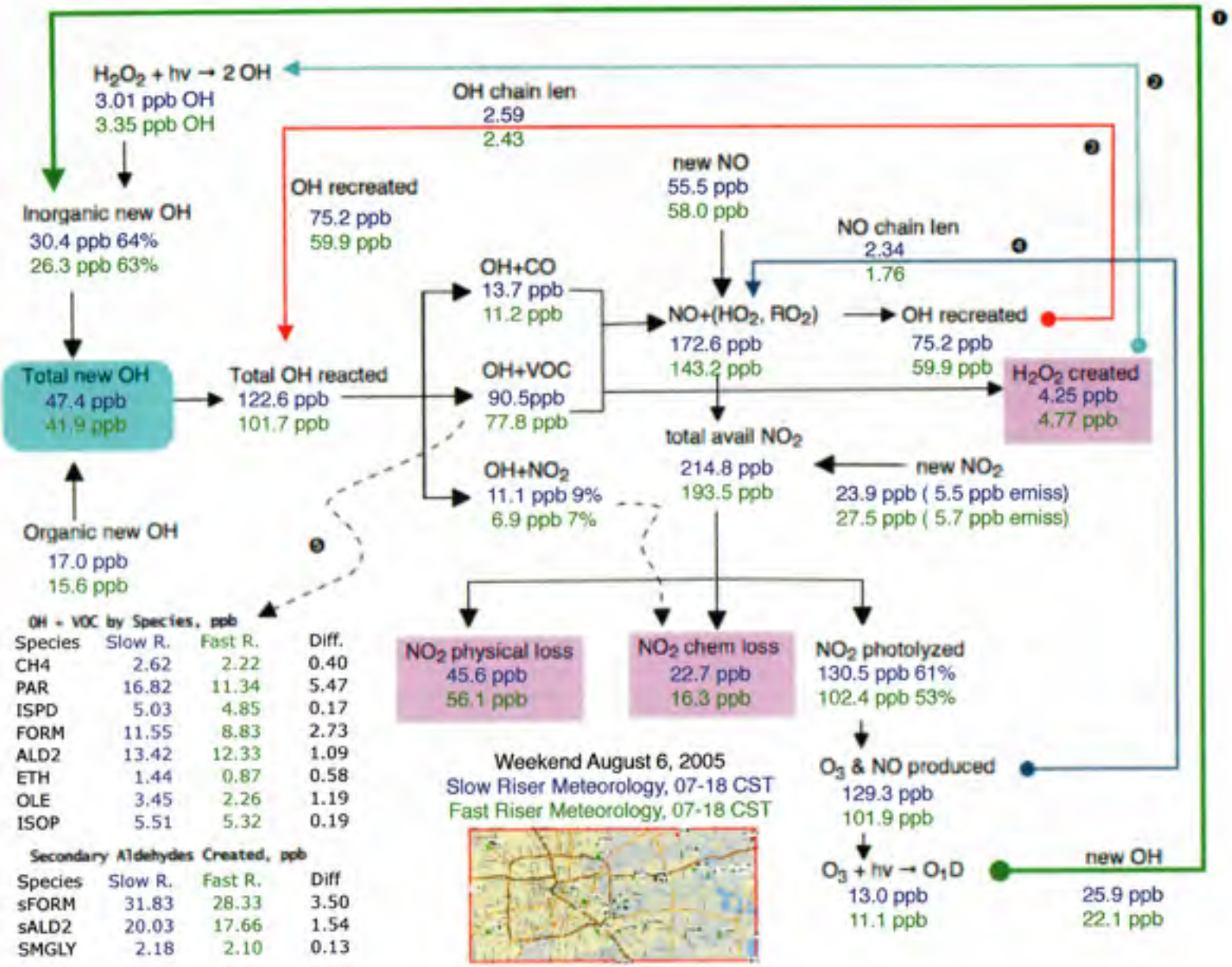

Figure C.5: OH cycle diagram and other chemical parameters of the weekend EI for slow riser (blue) and fast riser (green) summed over hours 8-18 LST. All values are in ppb unless denoted by a percentage.